JGP Journal of General Physiology

RESEARCH ARTICLE

Phosphoinositides modulate the voltage dependence of two-pore channel 3

Takushi Shimomura[1,2] and Yoshihiro Kubo[1,2]

Two-pore channels, or two-pore Na^+ channels (TPCs), contain two homologous domains, each containing a functional unit typical of voltage-dependent cation channels. Each domain is considered to be responsible for either phosphoinositide (PI) binding or voltage sensing. Among the three members of the TPC family, TPC1 and TPC2 are activated by $PI(3,5)P_2$, while TPC3 has been thought not to be affected by any PIs. Here, we report that TPC3 is sensitive to $PI(3,4)P_2$ and $PI(3,5)P_2$, but not to $PI(4,5)P_2$, and that the extremely slow increase in TPC3 currents induced by depolarization in *Xenopus* oocytes is due to the production of $PI(3,4)P_2$. Similarly to TPC1, the cluster of basic amino acid residues in domain I is critical for PI sensitivity, but with a slight variation that may allow TPC3 to be sensitive to both $PI(3,4)P_2$ and $PI(3,5)P_2$. We also found that TPC3 has a unique PI-dependent modulation mechanism of voltage dependence, which is achieved by a specific bridging interaction between domain I and domain II. Taken together, these findings show that TPC3 is a unique member of the TPC family that senses PIs and displays a strong coupling between PI binding and voltage-dependent gating.

Introduction

Two-pore channels or two-pore Na^+ channels (TPCs) have two homologous repeats of six-transmembrane helices (IS1–IS6 and IIS1–IIS6; Peiter et al., 2005; Calcraft et al., 2009). Each of the repeats is a functional unit containing a voltage sensor domain (VSD) and a pore domain, which are commonly observed in the superfamily of voltage-gated cation channels (Yu and Catterall, 2004). As four units form one functional channel in this superfamily, TPCs function as dimers (Guo et al., 2016; Kintzer and Stroud, 2016). In VSDs in general, basic amino acid residues that appear at every third position in helix S4 are essential for voltage sensing (Armstrong et al., 1974; Aggarwal and MacKinnon, 1996; Seoh et al., 1996). Although these basic residues are retained in both of the two VSDs in TPCs (VSD1 and VSD2), the number and the positions are different between the two VSDs and also between TPC subtypes. Animal TPCs were initially characterized as nicotinic acid adenine dinucleotide phosphate–dependent Ca^{2+} release channels (Brailoiu et al., 2009; Calcraft et al., 2009; Zong et al., 2009), but recent electrophysiological analyses have reported that they are activated by a type of phosphoinositide (PI), which is a minor phosphatidylinositol bisphosphate (PIP_2) species, $PI(3,5)P_2$, and are highly Na^+-selective channels (Wang et al., 2012; Cang et al., 2013, 2014b). Therefore, the ligands and the permeating ion species of TPCs are still under debate.

The TPC family has three members, each of which has a different localization and biophysical properties. TPC1 and TPC2 are localized in endosomes and lysosomes (Xu and Ren, 2015), and are important for the physiological aspects related to these intracellular organelles, such as autophagy (Lin et al., 2015; García-Rúa et al., 2016), mammalian target of rapamycin (mTOR)–dependent nutrient sensing (Cang et al., 2013), and Ebola virus infection (Sakurai et al., 2015). While TPC1 requires both voltage and $PI(3,5)P_2$ stimuli for opening, TPC2 is simply a $PI(3,5)P_2$-activated channel. Recent cryo-EM structures of mouse TPC1 (MmTPC1), with or without $PI(3,5)P_2$, revealed that $PI(3,5)P_2$ is bound to the regions containing the IS4-S5 linker and IS6 in domain I (She et al., 2018). The critical importance of this region was also verified in the action of nicotinic acid adenine dinucleotide phosphate (Patel et al., 2017). Mutagenesis studies showed that the positive charges in IS4 do not affect voltage sensing, but those in IIS4 do. Taken together with the structural analyses, these findings suggest that the two domains are specialized for each stimulus, namely, domain I for PIs and domain II for voltage.

In contrast to TPC1 and TPC2, fewer studies of TPC3 are reported, in either biophysical or physiological aspects. TPC3 is localized in the plasma membrane and in cortical granules in starfish oocytes (Ramos et al., 2014). It is evolutionally conserved

[1]Division of Biophysics and Neurobiology, National Institute for Physiological Sciences, Okazaki, Japan; [2]Department of Physiological Sciences, School of Life Science, The Graduate University for Advanced Studies (SOKENDAI), Hayama, Japan.

Correspondence to Takushi Shimomura: shimot@nips.ac.jp.

from echinoderms, such as sea urchins, to some mammals, but is lacking in primates and some rodents (Brailoiu et al., 2010; Cai and Patel, 2010). TPC3 has been believed not to be activated by any PIs, but to be simply a voltage-dependent Na^+-selective channel (Cang et al., 2014a). Characteristically, when TPC3 is expressed in the *Xenopus laevis* oocyte expression system, a long depolarizing step pulse generates slowly developing currents that last >10 s, by a so-called "induction" mechanism (Cang et al., 2014a).

PIs, especially three types of PIP_2, serve as important cofactors for membrane proteins (Balla, 2013). The regulatory roles of $PI(4,5)P_2$ on the activity and trafficking of many ion channels and transporters are well known. $PI(3,5)P_2$ is, so far, known to activate only two families of ion channels that are localized in endosomal and lysosomal membranes, namely transient receptor potential channel mucolipin 1–3 (TRPML 1–3), TPC1, and TPC2 (Dong et al., 2010; Wang et al., 2012; Cang et al., 2014b). The third type of PIP_2, $PI(3,4)P_2$, is considered to be localized mainly in the plasma membrane and early endosomes (Posor et al., 2013). $PI(3,4)P_2$ is produced by PI3-kinase (PI3K) from PI(4)P, as is Phosphatidylinositol (3,4,5)-trisphosphate (PIP_3), which is also known to be an important signaling PI, as represented by Akt activation (Manning and Toker, 2017). Although $PI(3,4)P_2$ has received less attention, several emerging pieces of evidence have indicated the unique and critical importance of $PI(3,4)P_2$, such as in spatially localized PI3K signaling (Braccini et al., 2015), endocytosis (Posor et al., 2013; Boucrot et al., 2015), neuronal death (Sasaki et al., 2010), membrane ruffling (Hogan et al., 2004), and cell migration (Bae et al., 2010; Li et al., 2016). $PI(3,4)P_2$ has been known to bind some membrane-associated proteins (Hogan et al., 2004; Li and Marshall, 2015). However, despite the physiological importance of $PI(3,4)P_2$, there are few reports of transmembrane proteins, including ion channels and transporters, that respond specifically to $PI(3,4)P_2$.

We investigated the molecular mechanism of induction of TPC3 using the two-electrode voltage clamp technique in the *Xenopus* oocyte expression system. By analysis of the induction, we newly found that the induction is caused by modulation of voltage dependence by $PI(3,4)P_2$, which is produced by the endogenous system in *Xenopus* oocytes. The application of PI to inside-out patches revealed that TPC3 is sensitive to both $PI(3,4)P_2$ and $PI(3,5)P_2$, but not to $PI(4,5)P_2$. We also identified the key amino acid residues for the coupling of PI binding with voltage-dependent gating, which is not observed in the case of $PI(3,5)P_2$ binding to TPC1. Our findings revealed features of the PI dependence and PI-dependent modulatory mechanism of TPC3 that are unique among the TPC family, providing us with insight into subtype-specific differences.

Materials and methods

Ethical approval

All animal experiments were approved by the Animal Care Committee of the National Institutes of Natural Sciences (an umbrella institution of National Institute for Physiological Sciences, Tokyo, Japan).

Reagents

All soluble analogues of PIs, such as $PI(3,4)P_2$-diC8, were purchased from Echelon Biosciences and dissolved in water as a 0.2-mM concentration of stock solution. PI stock solutions were directly used for PI injection experiments and diluted into the bath solution for inside-out patch experiments. Insulin (Wako) was dissolved in 10 mM HCl solution and kept as a 1-mM stock solution. Thapsigargin (Sigma-Aldrich) and wortmannin (Wako) were dissolved in DMSO at 1 mM and 10 mM for stock solution, respectively.

Complementary RNA (cRNA) preparation and injection into *Xenopus* oocytes

The complementary DNA (cDNA) of TPC3 from *Xenopus tropicalis* (XtTPC3; XP_002940387) in pUC57-Simple was synthesized by Genscript with one base replacement (T1395 to C) from original cDNA (GenBank accession no. XM_002940341) for abolishing the endogenous NdeI site (provided by Y. Fujiyoshi, Nagoya University, Nagoya, Japan). The XtTPC3 cDNA fragment was digested by cleavage at the NdeI and XhoI sites, which were attached at the 5′ and 3′ ends of XtTPC3 cDNA in pUC57-Simple, extracted, and blunted by the Klenow fragment. The fragment was then inserted to the SmaI site of the pGEMHE vector. A TAG sequence on the 3′ side of the SmaI site of the pGEMHE vector was used as a stop codon. The *Ciona intestinalis* voltage-sensitive phosphatase (Ci-VSP) cDNA was provided by Y. Okamura (Osaka University, Osaka, Japan). The cDNAs of fluorescent reporters sensitive to $PI(4,5)P_2$ (F-PLC) and $PI(3,4)P_2$ (F-TAPP) were provided by E.Y. Isacoff (University of California, Berkeley, Berkeley, CA). Site-directed mutagenesis was accomplished by a PCR-based method using PrimeSTAR Max DNA Polymerase and the In-Fusion HD Cloning Kit (Takara Bio), following the manufacturer's method. The plasmid sequences were confirmed by DNA sequencing. The cRNAs were synthesized with a mMESSAGE mMACHINE T7 kit (Ambion; Life Technologies) from the linearized cDNA.

Preparation and injection for *Xenopus* oocytes were performed as described previously (Kume et al., 2018). *X. laevis* for oocytes were purchased from Hamamatsu Seibutsu Kyouzai (Japan). The oocytes were collected from frogs anesthetized by 0.15% tricaine. The isolated oocytes were treated with 2 mg/ml collagenase (Sigma-Aldrich) for 6.5 h and stocked overnight or longer at 17°C in frog Ringer's solution containing (in mM) 88 NaCl, 1 KCl, 2.4 $NaHCO_3$, 0.3 $Ca(NO_3)_2$, 0.41 $CaCl_2$, 0.82 $MgSO_4$, and 15 HEPES, pH 7.6, with 0.1% penicillin–streptomycin (Sigma-Aldrich). Then, the oocytes were injected with 50 nl of cRNA solution and incubated at 17°C in frog Ringer's solution. The amount of injected cRNAs of XtTPC3 was 25 ng. In the case of coexpression experiments with Ci-VSP, 20 ng of XtTPC3 cRNA and 5 ng of Ci-VSP cRNA were mixed and injected. For fluorescent recording, 20 ng of XtTPC3 cRNA and 5 ng of Ci-VSP cRNA were mixed with 25 ng of F-PLC cRNA or 12.5 ng of F-TAPP. In the recording without Ci-VSP, 20 ng of XtTPC3 was mixed with 25 ng of F-PLC or 6.25 ng of F-TAPP. Currents were measured 2–6 d after injection, depending on the required current amplitude.

Two-electrode voltage clamp recording of oocytes

Currents were recorded under two-electrode voltage clamps using an OC-725C amplifier (Warner Instruments) and pClamp10.7 software (Molecular Devices). Data from the amplifier were digitized at 0.1 to 10 kHz, depending on recording protocols, through Digidata1440 (Molecular Devices), and digitally filtered at 100 Hz. The resistance of microelectrodes was adjusted to be 0.2–0.5 MΩ when filled with a solution of 3 M K-acetate and 10 mM KCl. The standard recording bath solution was ND-96, which contains (in mM) 96 NaCl, 2 KCl, 1.8 $CaCl_2$, 1 $MgCl_2$, and 5 HEPES, pH 7.4. Mes, pH 4.6, was used for low pH solutions. Unless especially noted, oocytes were held at −60 mV.

The membrane potential of oocytes expressing a large amount of XtTPC3 often increased above 0 mV in the ND-96 solution, thought to be caused by the autonomous induction and sustained opening of XtTPC3. Once XtTPC3 is activated, it slightly depolarizes the membrane potential toward the Na^+ reversal potential and thus causes further opening of XtTPC3, like the firing of an action potential. The noninactivating property of XtTPC3 facilitates and sustains the depolarized condition, and finally induces cell death of the oocytes. This problem was frequently encountered when Ci-VSP was coexpressed, as it potentiates XtTPC3. To avoid this fatal effect, the oocytes were often incubated in a low or medium Na^+ concentration solution instead of ND-96, where 96 mM NaCl was replaced with 10 mM NaCl and 86 mM NMDG-HCl (low) or with 18.6 mM NaCl and 77.4 mM NMDG-HCl (medium). The half-activation voltage ($V_{1/2}$) value of XtTPC3 WT was confirmed to be apparently not affected by this solution replacement.

To compare the conductance–voltage (G–V) relationship before and after induction, as in Fig. 1, C and D, a series of step pulses were given before and after the 80-mV pulse for 20 s. On recording of the current traces before induction, the −60 mV holding potential was sustained between step pulses to maintain the state before induction, generally for 1 min, and 15 or 30 s for the mutants, which show less induction. A 100-mV pulse for 50 ms before each step pulse, followed by returning to −60 mV, was given to confirm that the condition before induction is maintained. Otherwise, the currents would become gradually larger with the progress of step pulses. The step pulses were given from 10 mV to 200 mV for 50 ms, followed by 60-mV pulses for tail currents. On recording of the current traces after induction, the 100-mV depolarizing pulses for 500 ms, followed by returning to −60 mV, were given before each step pulse to maintain the induced condition with minimal interpulse interval. The step pulses were given from −20 mV to +170 mV for 50 ms, followed by 60-mV pulses for tail currents.

For the wortmannin or insulin pretreatments, the oocytes were incubated in the ND-96–based low Na^+ solution containing 30 µM wortmannin or 10 µM insulin for >1 h.

PI injection into *Xenopus* oocytes

In the PI injection experiments shown in Fig. 8, the water containing PIs was manually injected by positive pressure from a glass pipette. The injection of 0.2 mM $PI(4,5)P_2$–diC8 (Echelon Biosciences), the soluble derivative of $PI(4,5)P_2$, into the oocytes evoked the endogenous Ca^{2+}-activated Cl^- channel (CaCC) currents, which are thought to be caused by Ca^{2+} release through the soluble $PI(4,5)P_2$–activated inositol trisphosphate (IP_3) receptor. To abolish contamination by the Cl^- currents, the oocytes expressing XtTPC3 for $PI(4,5)P_2$–diC8 injection were pretreated with Ca^{2+}-free ND-96 (in mM: 96 NaCl, 2 KCl, 5 $MgCl_2$, 5 HEPES, pH 7.4, and 1 EGTA) containing 1 µM thapsigargin for >1.5 h, and then the current recording and PI injection were performed in the Ca^{2+}-free ND-96 solution. The time constant of activation at 100 mV was quantified as a parameter to reflect the PI-dependent change of voltage dependence. Furthermore, to verify no residual contamination of CaCC currents, which have similar kinetics to XtTPC3 currents at 100 mV, the current amplitude at 50 mV was also monitored. The appearance of inward currents at 50 mV was a good parameter of potentiation of XtTPC3, because the Cl^- currents would appear as outward currents at this membrane voltage. Also, XtTPC3 showed almost no currents because of its low open probability in the condition before induction. In addition, voltage ramps following the 50- and 100-mV test pulses were also monitored to verify that the reversal potential was not significantly altered by the leak caused by PI-induced oocyte swelling nor by contamination with CaCC currents. For the injection of PIs with lower activity for the IP_3 receptor than that of $PI(4,5)P_2$, the oocytes were pretreated with frog Ringer's solution containing 10 µM BAPTA-AM (Funakoshi) for ≥1.5 h to chelate the leaked Ca^{2+}. The recording and PI injection were performed in the Ca^{2+}-free ND-96 solution.

The aforementioned pulse stimulus from −30 mV holding potential was applied every 100 s, and the injection of 0.2 mM PIs was performed 100 s after the start of the recording. After 700 s, 80-mV depolarizing pulses were applied twice for 10 s, separated by a brief return to the holding potential as an induction stimulus. The current amplitude evoked by a 50-mV pulse at each step was normalized to that obtained after the induction stimulus. The time course of activation at 100 mV was fitted with a single exponential function. In some batches of oocytes, and especially in oocytes kept for several days, the kinetics were often fast, even before PI injection. This might have been caused by an increased $PI(3,4)P_2$ concentration. To detect the effects of PI injection clearly, oocytes kept for <2 d after injection and showing a time constant for activation >70 ms at 100 mV were chosen for PI injection experiments.

Recordings in inside-out patches from *Xenopus* oocytes

The oocytes were kept for >4 d in ND-96 solution with the medium Na^+ concentration. Immediately before the experiments, the oocytes were incubated in a hypertonic medium (in mM: 192 NMDG-HCl, 4 KCl, 3.6 $CaCl_2$, 2 $MgCl_2$, and 10 HEPES-NaOH, pH 7.4) for 10–15 min. The vitelline membrane was manually removed using forceps, and then the oocytes were transferred to, and again kept in, the ND-96 solution with medium Na^+ concentration. The glass pipettes were filled with ND-96 solution, and the resistance was 1–3 MΩ. Inside-out patches were excised from oocytes that had been transferred into the bath solution (in mM: 92 KCl, 10 NaCl, 0.5 $MgCl_2$, 1 EGTA, 0.5 K_2ATP, and 5 HEPES, pH 7.4). Currents were recorded using an AXOPATCH 200B amplifier (Axon Instruments) and pClamp10.8 software (Molecular Devices).

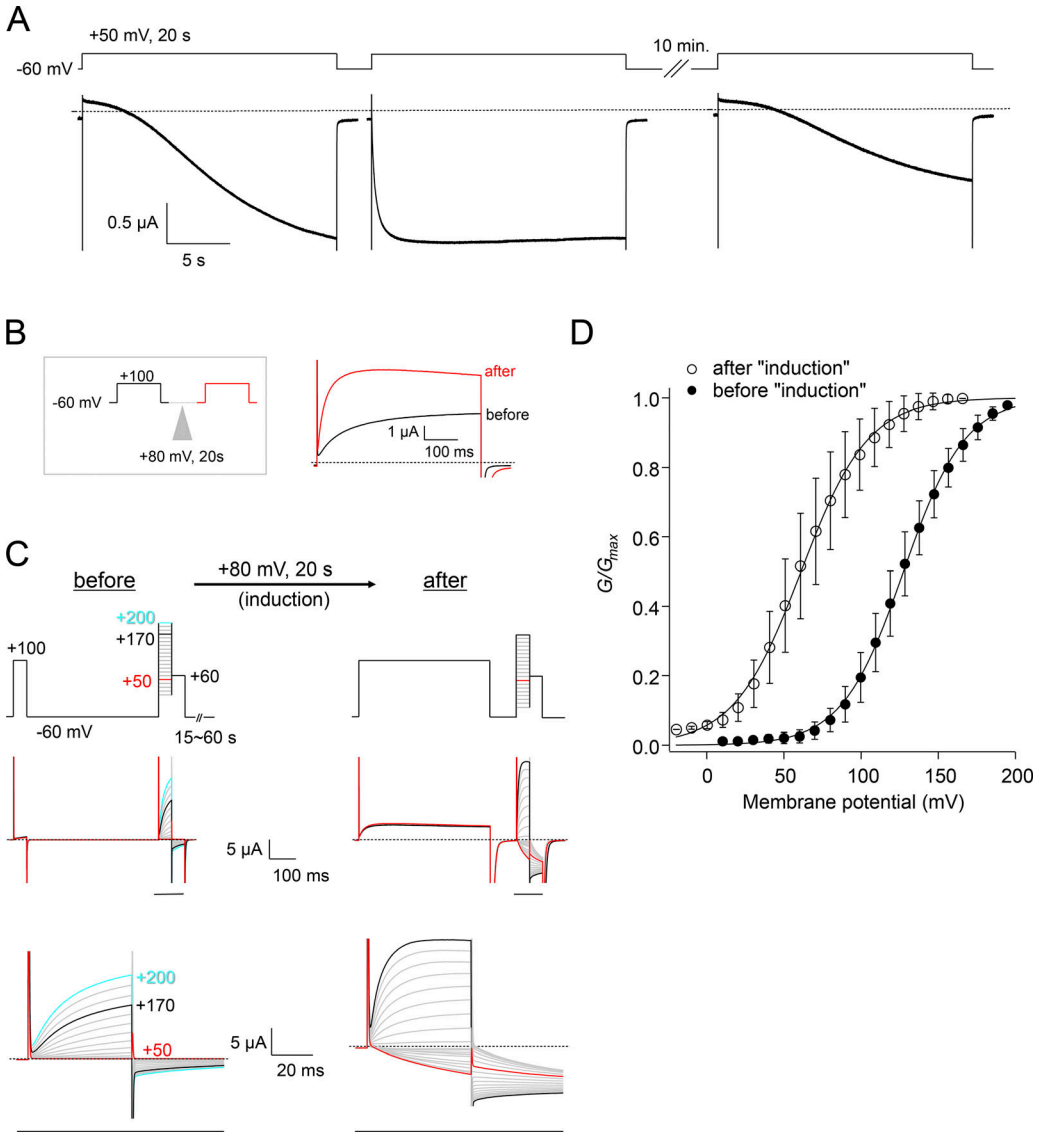

Figure 1. **Depolarization-induced modulation of the voltage dependence of XtTPC3 expressed in *Xenopus* oocytes. (A)** A representative current trace of induction of XtTPC3 in *Xenopus* oocytes. Currents were elicited by changing the membrane voltage from −60 mV holding potential to 50 mV for 20 s. Two sequential stimuli were applied, and then membrane voltage was maintained at the holding potential for 10 min until the third stimulus. **(B)** A brief protocol to check the extent of induction (left) and the resultant current traces of XtTPC3 before (black) and after (red) the induction stimulus of 80 mV for 20 s. **(C)** The protocol used to record the G–V relationships (top) and the resultant current traces (middle). The region indicated by a black bar is shown in an expanded view (bottom). Before induction, each step pulse was preceded by an interval of −60 mV holding potential, generally for 1 min, to maintain the channels in a pre-induction state. The interval time was varied depending on the mutant under study. To confirm that the channels were in a pre-induction state, the current amplitude elicited by a 100 mV pulse for 50 ms was monitored, to confirm stability of the amplitude within a series of sweeps. After a set of traces was obtained, an 80-mV depolarizing pulse was applied for 20 s, and then the current traces after induction were obtained. In the case after induction, to maintain the induced condition, 100-mV prepulses were applied for 500 ms before each step pulse. **(D)** G–V relationships of XtTPC3 before (filled) and after (open) induction. G/G_{max} is the normalized tail current amplitude. Error bars represent the SD of six independent experiments.

Data from the amplifier were digitized through Digidata1440 (Molecular Devices) at 4 kHz. PIs were applied using a Perfusion Fast-Step System (SF-77B; Warner Instrument).

Modeling of the XtTPC3 structure

A homology model of XtTPC3 was generated based on the cryo-EM structure of MmTPC1 bound with $PI(3,5)P_2$ (PDB accession no. 6C9A) using SWISS-MODEL (Schwede et al., 2003). The resultant XtTPC3 model, where the PI molecules were not included, was aligned with the original MmTPC1 structure using PyMol software (Delano Scientific). $PI(3,5)P_2$ molecules in the MmTPC1 structure were manually modified to $PI(3,4)P_2$ molecules and shown with the aligned XtTPC3 structure.

Fluorescent measurement using F-TAPP and F-PLC

Fluorescent detection of $PI(3,4)P_2$ and $PI(4,5)P_2$ levels, using the FRET-based probes F-TAPP and F-PLC, and data analysis were conducted as previously reported (Grimm and Isacoff, 2016).

Fluorescence was detected using a fluorescence microscope through a 20× 1.0 numerical aperture (NA) objective (Olympus XLUMPLFLN 20X), with a xenon lamp (Hamamatsu Photonics) as the light source. Light intensity was diminished to 25% through a neutral density filter. The cyan fluorescent protein (CFP) fluorescence was excited by light passed through a band-pass excitation filter (426–450 nm). The emitted light was passed through a filter (460-nm longpass) and divided by a dichroic mirror (505 nm). The intensities of shorter wavelength light, passed through a 430–490-nm filter, were detected as CFP signal, and those of longer wavelength, passed through a 510–55-nm filter, were detected as YFP signal. The two fluorescence signals were obtained by Photomultipliers (Hamamatsu Photonics). Current and fluorescent signals were simultaneously digitized and recorded through a Digidata 1322A and pClamp10.8 software (Molecular Devices). The YFP and CFP signals were sampled at 0.2 kHz and low pass filtrated for the analysis. A slow bleaching was adjusted by assuming that the decrease until the first voltage pulse was linear. The FRET values were obtained by dividing the YFP signal by the CFP signal. The baseline signal was normalized as 1.0, and the difference from the baseline was calculated as ΔFRET.

Data analysis and statistics

Electrophysiological data were analyzed using Clampfit 10.7 (Molecular Devices) and Igor Pro (WaveMetrics). Tail current amplitude elicited by +60 mV after step pulses was used to obtain G–V relationships. The G–V relationships were calculated by fitting to a two-state Boltzmann equation,

$$G = G_{min} + (G_{max} - G_{min})/(1 + e^{-zF(V-V_{1/2})/RT}),$$

where G indicates the conductance, and G_{max} and G_{min} are the maximum and minimum conductance, respectively. V is the membrane voltage, and $V_{1/2}$ is the half-activation voltage. z, F, R, and T are the effective charge, Faraday's constant, Gas constant and temperature, respectively. The normalized G/G_{max} was plotted as a function of membrane voltage.

To analyze the effects of Ci-VSP coexpression, as shown in Fig. 4, time constants for activation were obtained using Clampfit by fitting each trace with a single exponential function. In the coexpression experiments with Ci-VSP, the current traces at 100 mV showed an unusual development, and the time constants were apparently not fitted well by a single exponential function, possibly reflecting the mixed effects of Ci-VSP and XtTPC3 at 100 mV, such as Ci-VSP–dependent PIP_2 generation and the subsequent degradation, and the endogenous PIP_2 production capability of the *Xenopus* oocytes. The SEM of each fitting was at most 2% of the value of the time constants, which is far smaller than the change caused by the voltage difference in the presence of Ci-VSP. Therefore, despite of the inaccuracy of fitting, we used the time constants obtained by single exponential fitting as a parameter to indicate the change of the activation kinetics. The range of 200 ms after 100-mV depolarizing step pulses was used for fitting.

For the analysis of simultaneous recording of current and fluorescence, as shown in Fig. 7, the recordings of the initial 10 s after depolarizing step pulses were fitted to a double exponential function. Among current traces elicited by 30, 50, and 70 mV, those at 30 mV and 50 mV at increasing phase could not be fitted. This is possibly because the slower voltage-dependent activation becomes rate-limiting in the lower range of voltage and makes the time courses complicated. For this reason, only the traces of currents and fluorescence at 70 mV were used.

To analyze the effects of PI perfusion on XtTPC3 in the inside-out configuration, as shown in Fig. 9, the tail current elicited at −30 mV immediately after +80-mV pulses for 200 ms was used. The ratio of the current amplitude after and before PI perfusion was analyzed as fold increase of current amplitude.

Data are presented as mean ± SD. Student's t test was used to evaluate the $V_{1/2}$ before and after induction, the effects of PI injection on the time course, and the effects of wortmannin and insulin pretreatment. One-way ANOVA, followed by Dunnett's test, was used to estimate statistical significance in comparison of the increased current amplitude in multiple PI injection and mutational effects. One-way ANOVA, followed by Tukey's test, was used to evaluate the PI perfusion–induced fold increase of current amplitude in multiple comparison between groups. $P < 0.05$ was considered statistically significant.

Online supplemental material

Fig. S1 shows the combined effects of Ci-VSP coexpression and insulin pretreatment on the activation kinetics of XtTPC3. Fig. S2 shows the effects of thapsigargin pretreatment on the oocytes for $PI(4,5)P_2$ injection. Fig. S3 shows a series of G–V relationships of the XtTPC3 channels with mutations to the putative PI binding site. Fig. S4 shows the representative current recordings of the R187Q mutant coexpressed with Ci-VSP. Fig. S5 shows the effects of $PI(3,4)P_2$ injection to the oocytes expressing the R187Q mutant. Fig. S6 shows the comparison of MmTPC1 structures with or without $PI(3,5)P_2$.

Results

Modulation of voltage dependence of TPC3 by long depolarization in *Xenopus* oocytes

XtTPC3 was expressed in *Xenopus* oocytes. On application of two sequential 50-mV depolarizing pulses for 20 s, the first pulse generated slowly developing and noninactivating inward currents, but the second one showed clearly more rapid activation (Fig. 1 A). Then, after the oocyte was maintained at −60 mV holding potential for 10 min, another depolarizing pulse again generated the slowly increasing current. This induction by depolarization stimulus and recovery phenomenon suggests that some properties of XtTPC3 could be reversibly changed. As such a property, we investigated whether or not the voltage dependence was changed before and after induction. Comparison of G–V relationships shows that the voltage dependence was significantly shifted in the hyperpolarized direction after induction (Fig. 1, B–D; $V_{1/2}$ = 128 ± 8.4 mV before, 61.8 ± 13 mV after, n = 6). Considering this depolarization-induced shift of voltage dependence, induction is explained as a gradual increase in the open probability of noninactivating XtTPC3 by the sustained depolarizing pulse, which appears as a slowly developing increase in the current amplitude.

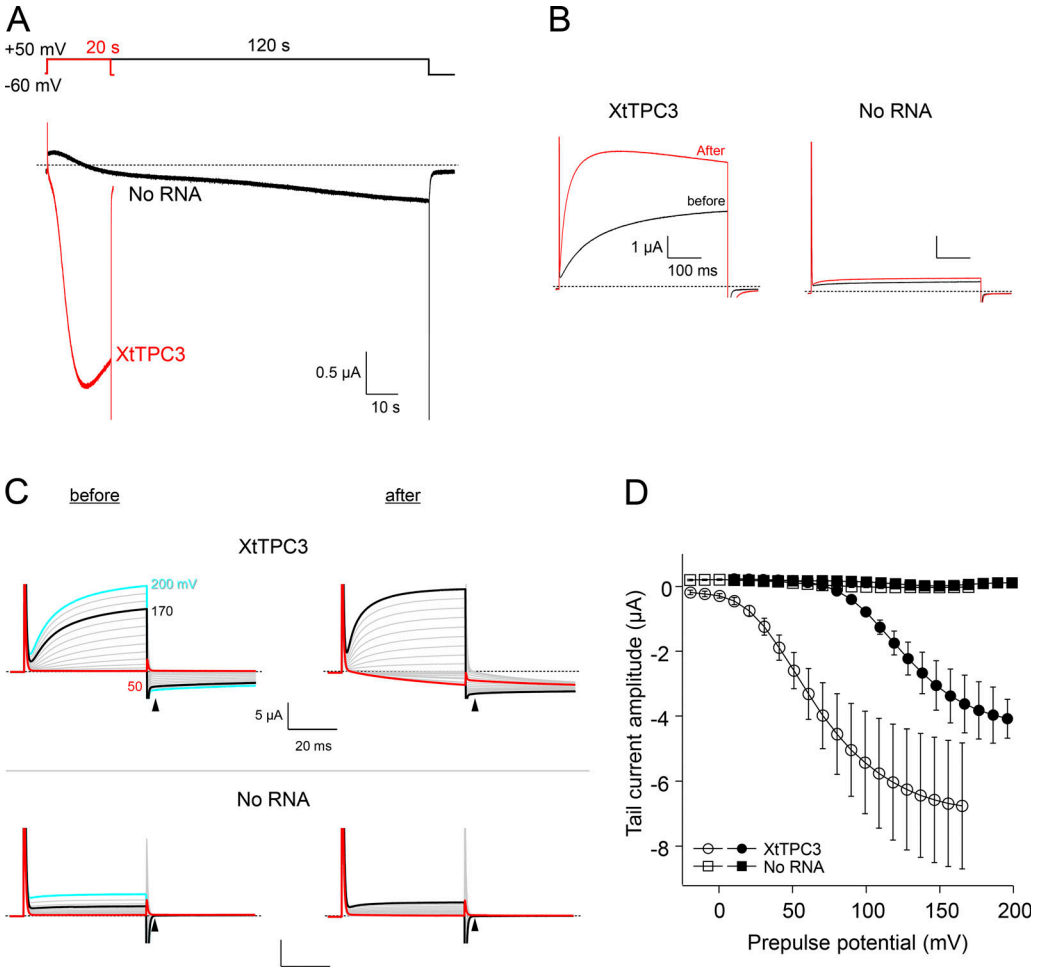

Figure 2. **Comparison of endogenous "inducible" Na^+ current and exogenously expressed XtTPC3 current recordings. (A)** Representative current traces obtained with a +50 mV long depolarizing pulse from oocytes with or without XtTPC3 cRNA injection. **(B)** Representative current traces obtained with a +100 mV depolarization pulse from the −60-mV holding potential before and after induction. Two traces from oocytes in which XtTPC3 cRNA was injected (left) or not injected (right) are shown. The induction stimulus was +80 mV for 20 s. **(C)** Representative current traces for obtaining G–V relationships. Currents were elicited by the same protocols as shown in Fig. 1 C. Traces from the same oocytes before (left) and after (right) induction are shown. Black arrows indicate the time points at which tail current measurements were made. **(D)** Plots of tail current amplitude versus prepulse voltage before (closed) and after (open) induction. Error bars represent the SD of five independent experiments.

Previous studies showed that *Xenopus* oocytes have a TPC3-like endogenous Na^+ conductance that is also increased by long depolarization (Baud et al., 1982; Cang et al., 2014a). These endogenous Na^+ currents are by far smaller and have much slower induction kinetics than the exogenously expressed XtTPC3 currents (Fig. 2, A and B). Comparison of the tail currents using the protocols to obtain G–V relationships showed that the tail current amplitudes at 60 mV from the oocytes without cRNA injection are negligible, compared with those from XtTPC3, both before and after induction (Fig. 2, C and D). For these reasons, we believe that, despite the endogenous Na^+ conductance, the results of our analyses reflect the exogenously expressed XtTPC3 activity.

Critical roles of PIs for the modulation of voltage dependence

We assumed that the shift of voltage dependence by long depolarization is caused by the PI dependence of XtTPC3. In a previous study, TPC3 was concluded to be insensitive to either $PI(3,5)P_2$ or $PI(4,5)P_2$ (Cang et al., 2014a), but it remains possible that other PIs are related to the induction. Consistent with this hypothesis, a pretreatment with wortmannin, a PI3K inhibitor that perturbs the PI production pathway, attenuated the depolarization-induced G–V shift (Fig. 3).

To confirm the involvement of PIs more directly, Ci-VSP (Murata et al., 2005) was coexpressed with XtTPC3. In response to depolarization, Ci-VSP dephosphorylates PIP_3 to $PI(3,4)P_2$ and $PI(4,5)P_2$ at lower membrane voltage, and even to PI(4)P at higher membrane voltage (Fig. 4 A; Grimm and Isacoff, 2016). During a 50-mV depolarizing pulse, XtTPC3 coexpressed with Ci-VSP showed a far faster current increase than that without Ci-VSP and was then followed by current decrease (Fig. 4 B). The protocol for obtaining the G–V relationship was difficult to be applied to the Ci-VSP coexpression experiment, because the prepulses with various membrane voltage change both the open probability of XtTPC3 and the Ci-VSP activity, making the G–V relationship ambiguous. Alternatively, we used

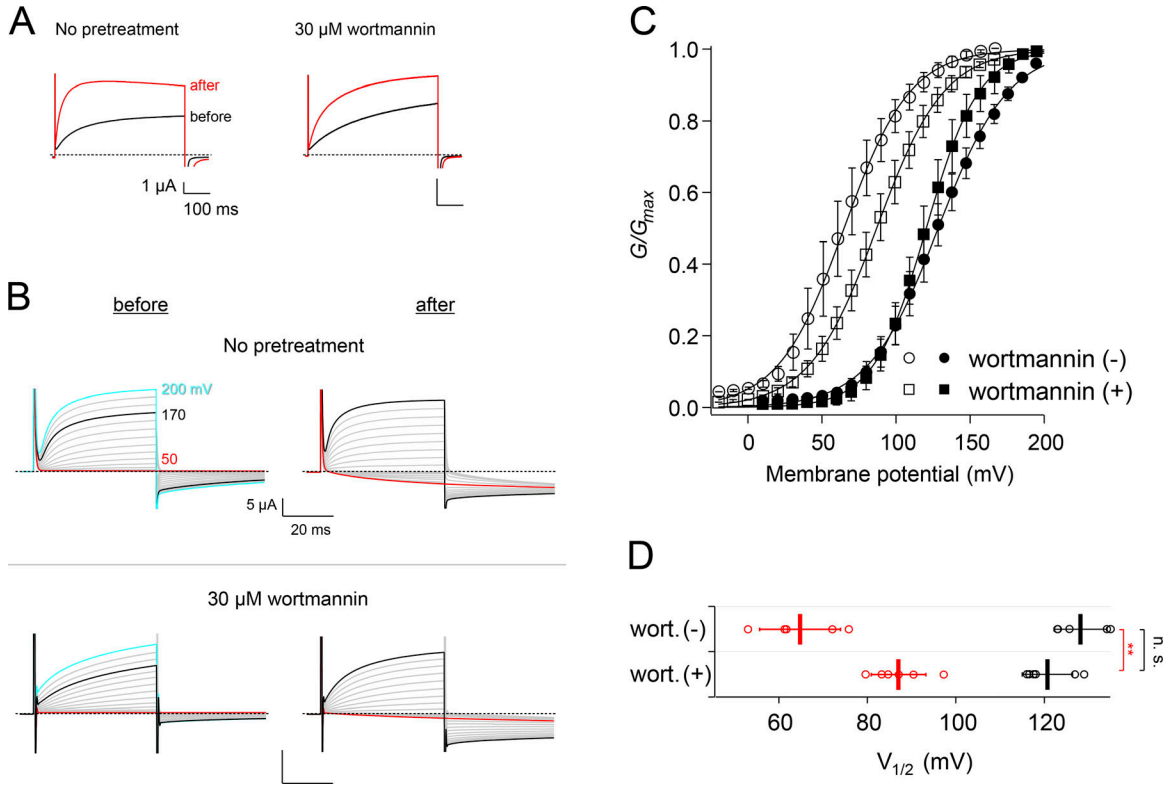

Figure 3. **The effects of wortmannin pretreatment on the G–V relationships before and after induction. (A)** Representative traces evoked by a 100-mV step pulse before (black) and after (red) induction. **(B)** Representative current traces from the 30 μM wortmannin-treated or nontreated oocytes for obtaining the G–V relationships. The currents before and after induction were elicited by the same protocols as Fig. 1 C, although the tail currents were obtained at 50 mV because of the small amplitude. The 100-mV prepulse in each condition was omitted for clarity. **(C)** G–V relationships of XtTPC3 with (square) or without (circle) wortmannin pretreatment. Data before (filled) and after induction (open) are shown. **(D)** Plots of $V_{1/2}$ before (black) and after (red) induction with or without wortmannin pretreatment. Error bars represent the SD of five to seven independent experiments. n.s., not significant at $P > 0.05$; **, $P < 0.01$. wort., wortmannin.

a two-pulse protocol, where the activity of Ci-VSP was evoked by prepulses to various membrane voltages, and then the effects on the time constant of activation were monitored by test pulses to 100 mV (Fig. 4 C). The relationship between time constant of activation and prepulse membrane voltage showed that the activation was accelerated by prepulses at around 30 mV and then decelerated by those at further higher membrane voltage (Fig. 4, D–G). This double mode of action, as well as the rapid current increase and subsequent decrease under the continuous depolarizing condition (Fig. 4 B), are considered to reflect the two steps of voltage-dependent activity of Ci-VSP (Fig. 4 A). These results indicate that XtTPC3 is potentiated, presumably by $PI(3,4)P_2$ and/or $PI(4,5)P_2$ that is produced at a depolarized potential at around 30 mV and degraded at a further higher membrane voltage by Ci-VSP.

A long depolarizing pulse is known to increase $PI(4,5)P_2$ and $PI(3,4)P_2$ concentration in a different voltage-dependent manner in the endogenous system of *Xenopus* oocytes (Zhang et al., 2010; Ratzan et al., 2011; Kurokawa et al., 2012; Grimm and Isacoff, 2016). The two-pulse protocol was used to evaluate the voltage dependence of induction, similar to the Ci-VSP coexpression experiment (Fig. 5). The relationship between time constant of activation and prepulse membrane voltage showed that the $V_{1/2}$ value of induction was 32.9 ± 2.7 mV (n = 6). The voltage dependence of $PI(3,4)P_2$ production by the endogenous mechanism, which is monitored by a $PI(3,4)P_2$-specific fluorescent sensor, appears over +10 mV (Kurokawa et al., 2012). On the other hand, the $V_{1/2}$ value of $PI(4,5)P_2$ production by a long depolarization, monitored by the $PI(4,5)P_2$ sensitivity of KCNQ2/3 channel, was calculated as −26.1 mV in a previous report (Zhang et al., 2010). Therefore, $PI(3,4)P_2$ is a more plausible cause for induction.

$PI(3,4)P_2$ potentiates XtTPC3 in *Xenopus* oocyte membrane

The contribution of $PI(3,4)P_2$ and/or $PI(4,5)P_2$ to XtTPC3 was further verified by several lines of experiments. First, the effects of the Ci-VSP F161W/R232K mutant, which is known to attenuate the dephosphorylation activity from $PI(3,4)P_2$ and $PI(4,5)P_2$ to PI(4)P (Grimm and Isacoff, 2016), were investigated. As expected, coexpression of XtTPC3 with Ci-VSP F161W/R232K attenuated the decreasing phase under continuous depolarization (Fig. 4 B) and abolished the deceleration of activation at highly depolarized voltage in the two-pulse protocol (Fig. 4, F and G). Second, oocytes expressing XtTPC3 were pretreated with insulin, which is known to increase $PI(3,4)P_2$ and PIP_3 concentration through endogenous PI3K activity (Liu et al., 1995; Grimm and Isacoff, 2016). To evaluate the potentiation of XtTPC3 by insulin, we used a 100-mV test pulse to monitor the time constant of

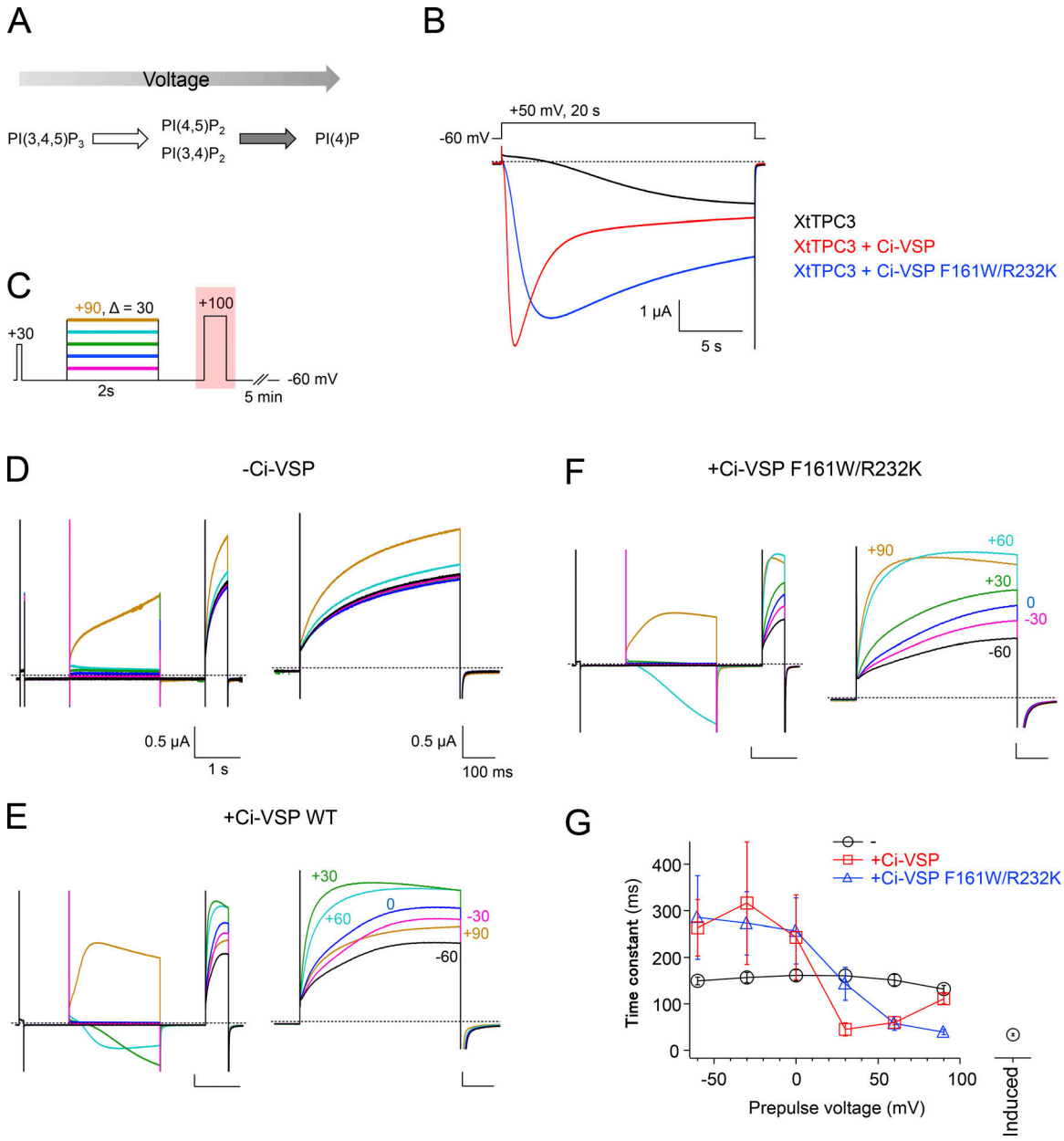

Figure 4. **Modulation of induction and activation kinetics of XtTPC3 by Ci-VSP. (A)** A scheme showing the voltage-dependent switch of the phosphatase activity of Ci-VSP. Ci-VSP dephosphorylates PIP_3 to $PI(3,4)P_2$ and $PI(4,5)P_2$ at lower membrane voltage, and even to PI(4)P at higher membrane voltage. **(B)** Representative current traces of XtTPC3 only (black), with Ci-VSP WT (red), or with Ci-VSP F161W/R232K (blue). **(C)** The protocol to obtain the voltage-dependent effects of Ci-VSP on time constants of activation in XtTPC3. The effect of a prepulse to various membrane voltages for 2 s, which is short enough not to cause the induction, was monitored during the subsequent 100-mV test pulse for 500 ms. To verify recovery to the basal condition after 5 min at holding potential, the current amplitude generated by a short 30-mV pulse was checked before the prepulses. **(D–F)** Representative current traces of XtTPC3 only (D), with Ci-VSP WT (E) and with Ci-VSP F161W/R232K (F). The whole traces elicited by the protocol in (C; left) and the partial traces elicited by 100 mV test pulse (right) are shown. **(G)** The relationships between time constants of activation and prepulse voltages. Time constants were obtained by fitting each trace with a single exponential function. The time constant labeled "induced" (the separate plot on the right) was obtained from the current traces evoked after a 20-s, 80-mV induction stimulus in WT. Error bars represent the SD of six independent experiments.

activation, and a 50-mV pulse for inward currents because the inward currents at 50 mV are a good indication of Na^+ influx in XtTPC3 (Fig. 6). The results showed that insulin pretreatment accelerates the activation kinetics at 100 mV and increases the current amplitude at 50 mV, which indicates the occurrence of potentiation of XtTPC3 even without induction stimulus. The insulin pretreatment of oocytes coexpressing XtTPC3 with Ci-VSP showed that time constants of activation at 30 mV are not further accelerated by insulin, which supports the notion that insulin potentiates XtTPC3 through PIP_3 and/or $PI(3,4)P_2$ production (Fig. S1).

Third, we compared the time course of the change in $PI(3,4)P_2$ and $PI(4,5)P_2$ concentration and of the induction progress, using $PI(3,4)P_2$- and $PI(4,5)P_2$-specific fluorescence sensor proteins

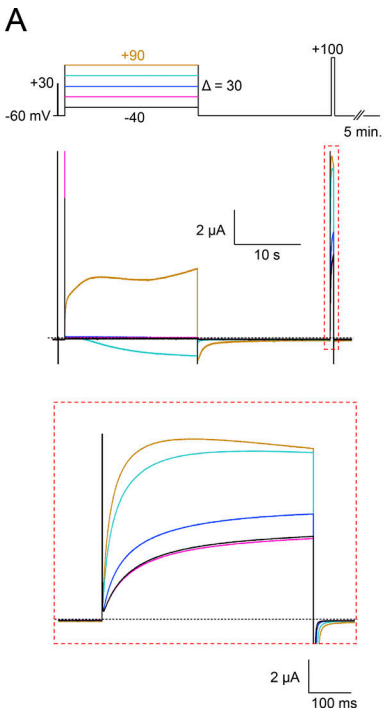

Figure 5. **Voltage dependence of induction. (A)** The protocol (top) and resultant representative current traces (middle) to obtain the voltage dependence of induction. The prepulses with different membrane voltage were given for 20 s, and then the membrane was kept at the holding potential for 20 s. The effect of the prepulses was monitored during the subsequent 100-mV test pulse. The currents evoked by 100-mV test pulses, in the red dotted box, are shown in an expanded view (bottom). **(B)** The relationship between time constant of activation and prepulse voltage, obtained from A. The current traces evoked by 100-mV test pulses were fitted by a single exponential function. $V_{1/2}$ (mV) is 32.9 ± 2.7 mV. Error bars represent the SD of six independent experiments.

(Grimm and Isacoff, 2016). XtTPC3 was coexpressed with Ci-VSP and F-TAPP or F-PLC, the FRET-based fluorescent reporters for PI(3,4)P_2 and PI(4,5)P_2, respectively, and the XtTPC3 current and FRET change (YFP/CFP) were simultaneously monitored. The normalized recording of FRET using F-TAPP showed a rapid increase and subsequent decrease (Fig. 7 A), which reflects the increase and decrease in PI(3,4)P_2 concentration as previously reported (Grimm and Isacoff, 2016). The pattern of FRET changes

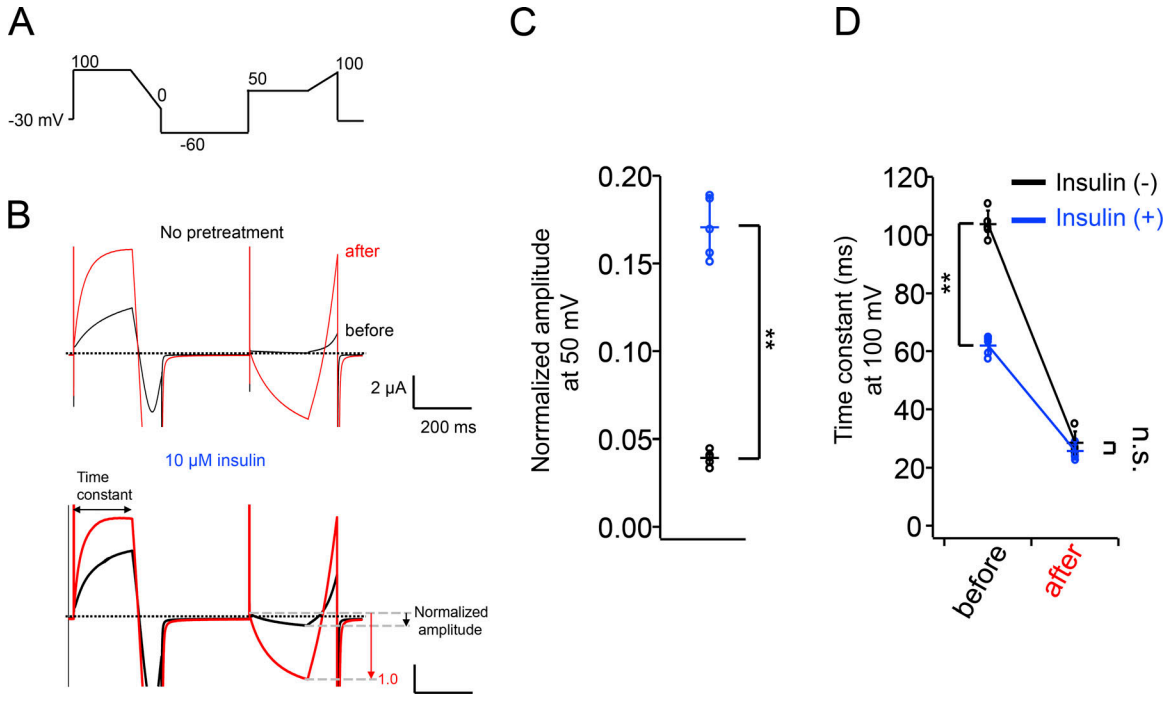

Figure 6. **The effects of insulin pretreatment on XtTPC3. (A)** The protocol for examining the potentiation of XtTPC3. **(B)** Representative current traces evoked by the protocol (A), without (top) or with (bottom) 10 μM insulin pretreatment. The pulse protocol was given before (black) and after (red) an induction stimulus (80 mV for 20 s). **(C)** The plot of normalized amplitude evoked by a 50-mV stimulus with (blue) or without (black) insulin pretreatment. The current amplitude before induction was normalized by that after induction as depicted in B. **(D)** The plot of time constant of activation at 100 mV. Error bars represent the SD of five independent experiments. n.s., not significant at $P > 0.05$; **, $P < 0.01$.

of F-TAPP is apparently consistent with that of XtTPC3 currents. A double exponential function was fitted only to the current traces at 70 mV, because it was not well fitted to the apparent multistep increasing phase at 30 mV and 50 mV (See also Materials and methods). Comparison of the time constants of increasing and decreasing components between current and fluorescence showed that they are similar in order of magnitude (Fig. 7 B). On the other hand, the time course of FRET change from F-PLC showed a continuous decrease over the voltage range tested, which is clearly different from the current traces (Fig. 7 C). In addition, even in the absence of Ci-VSP, we detected a FRET increase of F-TAPP, but not of F-PLC (Fig. 7, D–F). These results suggest that the increase in $PI(3,4)P_2$ concentration causes the induction, namely XtTPC3 potentiation.

Finally, a series of PIs was directly injected into the oocytes expressing XtTPC3, one at a time. The injection of a soluble derivative of $PI(4,5)P_2$ to oocytes evoked the endogenous Ca^{2+}-activated Cl^- currents that are thought to be caused by Ca^{2+} release through the soluble $PI(4,5)P_2$-activated IP_3 receptor (Fig. S2; Barish, 1983). Therefore, oocytes for $PI(4,5)P_2$ injection were pretreated with thapsigargin to deplete Ca^{2+} in the endoplasmic reticulum, and those for other PIs were incubated with BAPTA-AM to buffer the weak Ca^{2+} leak that occurs at high concentrations of PI injection. In addition, we used the same two parameters as shown in Fig. 6 A (Fig. 8 A), which are especially beneficial to minimize the residual contamination by the Cl^- current, because it appears as outward current at 50 mV while XtTPC3 shows inward current. Therefore, both the acceleration of activation kinetics at 100 mV and the increase in inward currents at 50 mV are appropriate for evaluation of XtTPC3 potentiation. Among all types of PIs, $PI(3,4)P_2$ was the most effective to accelerate the activation at 100 mV and to increase the currents at 50 mV, and PIP_3 was the second most effective (Fig. 8). The other PIs showed no significant potentiation effect. Considering the effects of Ci-VSP WT and F161W/R232K that indicated the potentiation by $PI(3,4)P_2$ increase, $PI(3,4)P_2$, rather than PIP_3, is thought to be the most potent XtTPC3 modulator among PI species in *Xenopus* oocyte membranes.

$PI(3,4)P_2$ and $PI(3,5)P_2$ potentiate XtTPC3 in inside-out patches of *Xenopus* oocytes

We next performed PI perfusion of inside-out patches from *Xenopus* oocytes expressing XtTPC3. Consistent with the PI injection experiments, $PI(3,4)P_2$ increased the XtTPC3 current (Fig. 9 A). The fold increase of the current amplitude by $PI(3,4)P_2$ application was significantly larger than that by $PI(4,5)P_2$, which clearly has no effects on XtTPC3 (Fig. 9, A and C). PIP_3 also tended to potentiate XtTPC3, although its effect is not significant. Unexpectedly, we found that $PI(3,5)P_2$ also potentiates XtTPC3 to an extent comparable to $PI(3,4)P_2$, which is inconsistent with the PI injection experiment (Fig. 8). The successive application of $PI(3,4)P_2$ and $PI(3,5)P_2$ to an inside-out patch clearly showed the potentiation effects of both PI species to XtTPC3 (Fig. 9 B). Given the results of direct PI injection in *Xenopus* oocytes, $PI(3,4)P_2$ is considered to be an effective ligand of XtTPC3 expressed in the plasma membrane. The apparent discrepancy in the results of Fig. 8 and Fig. 9 might be due to the preferable subcellular localization of injected $PI(3,5)P_2$ to organelle membranes, rather than the plasma membrane (Marat and Haucke, 2016), or due to any mechanisms in XtTPC3 and/or cytoplasm that perturb $PI(3,5)P_2$ sensitivity in the plasma membrane in whole oocytes.

The structural determinants of PI binding underlying induction in XtTPC3

Recent cryo-EM structures of MmTPC1 revealed the critical residues for $PI(3,5)P_2$ binding in domain I, which are located in the H1-IS0 loop in the N-terminal cytoplasmic region, IS3, the IS4-S5 linker, and IS6 (Fig. 10, A–C; She et al., 2018). Most of them are basic residues, such as arginines and lysines, that interact with negative charges of the phosphate groups of $PI(3,5)P_2$. Because many basic residues in these regions are also conserved in XtTPC3 (Fig. 10 C), we assumed that they form the $PI(3,4)P_2$ binding site and hence are important for induction. To gain insight into the structural basis of $PI(3,4)P_2$ recognition in XtTPC3, we built the MmTPC1 structure-based homology model, where $PI(3,5)P_2$ was simply replaced with a $PI(3,4)P_2$ molecule.

Mutations of the basic residues in the IS4-S5 linker and IS6 were found to affect the induction in a slightly different way from the case of MmTPC1 (Fig. 10, D–F; SI Appendix; and Fig. S3). In the IS4-S5 linker, mutations of both Arg187 and Arg191, whose corresponding arginines in MmTPC1 are essential to $PI(3,5)P_2$ binding, abolished the induction almost completely. It is notable that the mutations of Arg194 in the IS4-S5 linker and of Arg297 in IS6 also significantly attenuated the induction, although their corresponding residues are not conserved in TPC1 (Fig. 10 F and Fig. 11). Besides in the IS4-S5 linker and IS6, a basic residue in IS3 (Lys137 in XtTPC3 and Arg173 in MmTPC1) was also indispensable for both induction in XtTPC3 and $PI(3,5)P_2$ binding in MmTPC1. In contrast to domain I, neutralizing mutations of positively charged amino acid residues in domain II (IIS4-S5 linker and IIS6) did not show significant effects on induction (Fig. 10 F and Fig. S3).

Next, to prove that the residues important for induction actually contribute to $PI(3,4)P_2$ binding, the effects of Ci-VSP coexpression and $PI(3,4)P_2$ injection were investigated using R187Q, which was chosen as a representative mutant lacking induction. As expected, R187Q was less affected by Ci-VSP coexpression (Fig. 10 G and Fig. S4). Also, an injection of $PI(3,4)P_2$ into oocytes expressing R187Q showed no significant acceleration of the activation kinetics at 100 mV (Fig. S5). Furthermore, perfusion of either $PI(3,4)P_2$ or $PI(3,5)P_2$ failed to potentiate R187Q (Fig. 10, H and I). These results demonstrate that the basic residues responsible for induction form the $PI(3,4)P_2$ binding site in XtTPC3.

Difference in the putative recognition site for phosphate groups

In the H1-IS0 loop region of MmTPC1, a neutral residue (Asn85) was shown to be important for recognizing the C4 hydroxyl group of $PI(3,5)P_2$ (Fig. 12, A and B; She et al., 2018). We evaluated the effects of alanine mutations of three residues in the H1-IS0 loop of XtTPC3 (Asn52, Arg53, and Asn54) on induction (Fig. 12, C and D). In contrast to MmTPC1, alanine substitution of

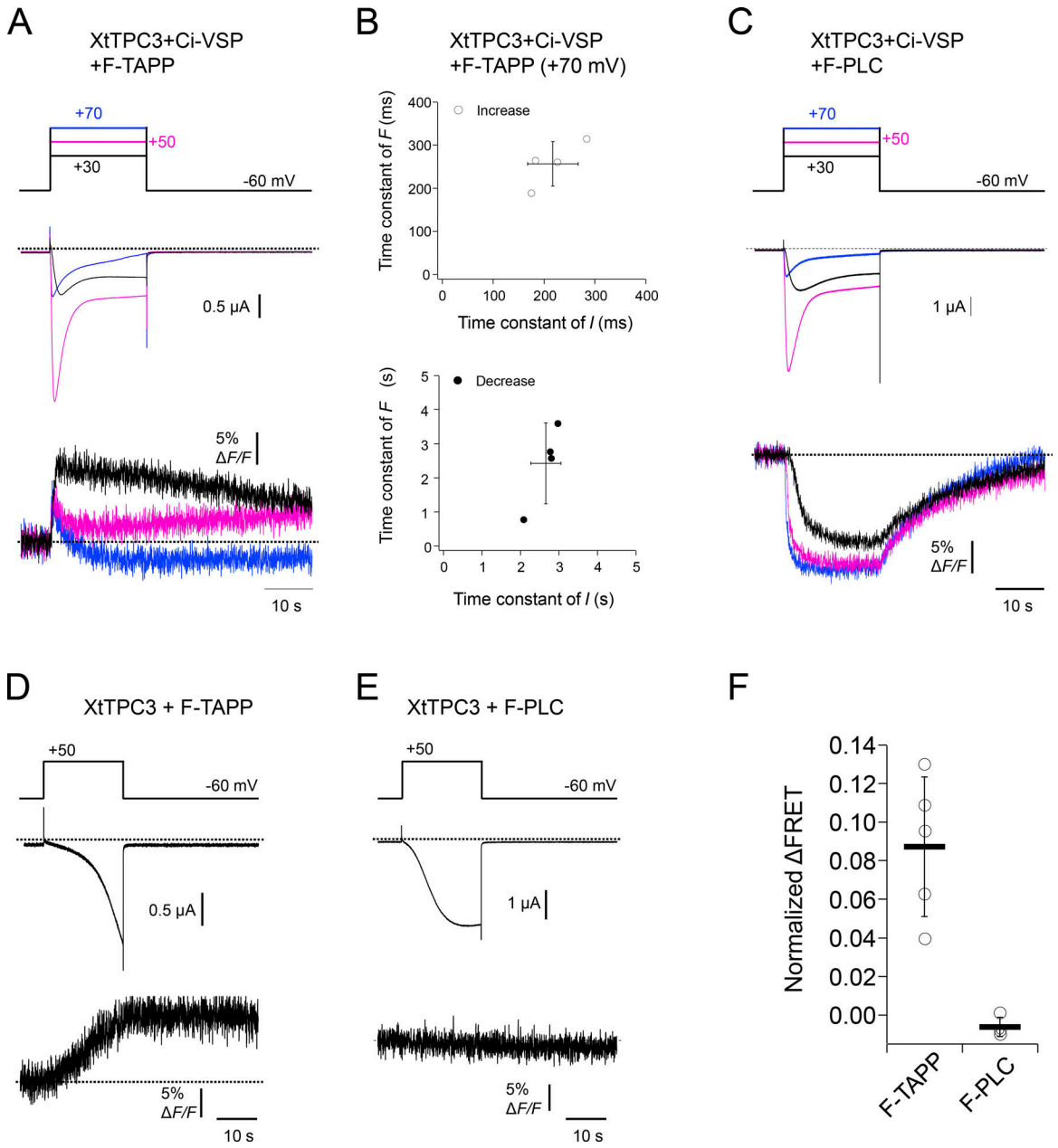

Figure 7. **Simultaneous recording of XtTPC3 currents and fluorescence signals of FRET-based PI sensors. (A and C)** Representative recordings of currents (middle) and fluorescence signals (bottom) elicited by step pulses (top), in XtTPC3 coexpressed with Ci-VSP and F-TAPP (A) or F-PLC (C). The current traces elicited by a 70-mV step pulse often appeared as inward currents, possibly because of a positive shift of the reversal potential caused by incubation in the low Na^+ solution. **(B)** Comparative plots of the time constants at 70 mV between current and fluorescence. The recordings of currents and fluorescence were fitted to a double exponential function, and the kinetics of the increasing (top) components and decreasing (bottom) components were compared between current and fluorescence. "*I*" and "*F*" in each axis indicate the current and fluorescence, respectively. **(D and E)** Representative recordings of currents (middle) and fluorescence (bottom) elicited by +50-mV step pulses (top), in XtTPC3 with F-TAPP (D) or F-PLC (E), without Ci-VSP. **(F)** Plots of the normalized peak value of ΔFRET as shown in D and E. Error bars represent the SD of four or five independent experiments.

Asn52, which corresponds to Asn85 in MmTPC1, did not show significant effects on induction, but alternatively, N54A did. The mutation of Arg53 revealed limited contribution of the basic residue at this position. The results indicate that Asn54, a neutral amino acid in a different position from TPC1, contributes to $PI(3,4)P_2$ recognition in XtTPC3.

As this region is considered to be responsible for the PI selectivity, we further evaluated the mutations of Arg53 and Asn54, including the replacement with those of TPC1. Various mutations of Asn54, including lysine, aspartate, glutamine, and threonine, failed to show an extent of induction comparable to WT (Fig. 12 D). These results indicate that the asparagine residue at this position is not replaceable for efficient $PI(3,4)P_2$-induced potentiation. In contrast, the lesser effects of both R53Q and R53A suggest a supplemental role for induction, while the reversed charge (R53D) was not permissive. R53D/N54K, in which

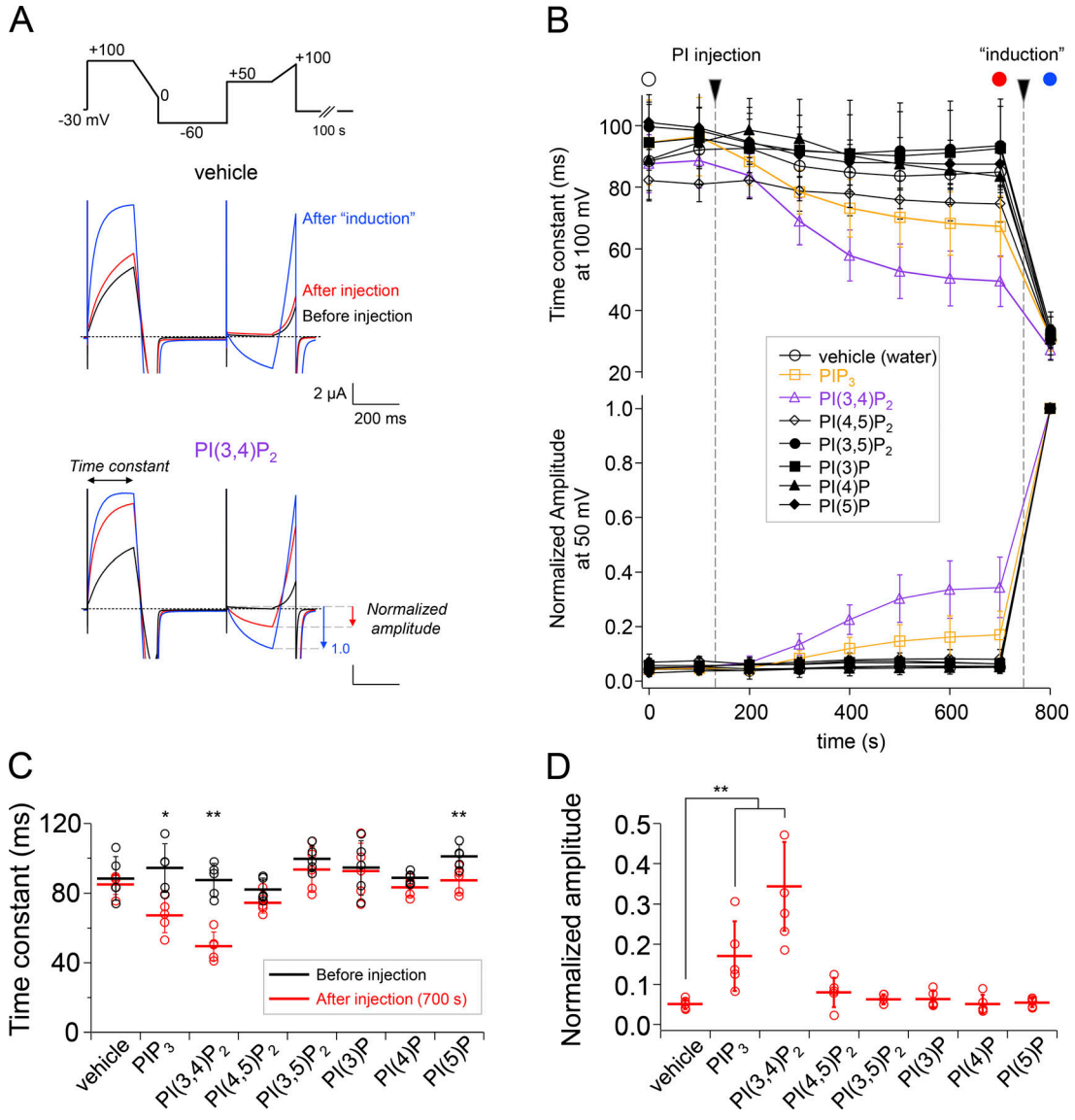

Figure 8. **Effects of PI injection in oocytes expressing XtTPC3. (A)** Representative current traces in the PI injection experiments. The protocol to obtain the two parameters at 50 mV and 100 mV (top), and representative current traces injected with water (middle) or 0.2 mM PI(3,4)P_2 (bottom) are shown. For each injection, the traces before injection (black; 0 s), after injection (red; 700 s) and after an induction stimulus (blue; 800 s) are shown. **(B)** Time courses of the effects of 0.2-mM PI injection on time constants of activation at 100 mV (top) and the amplitude of inward currents (bottom). PIs or water were injected after the second pulse. After the eighth pulse, the 80-mV depolarization stimulus was given twice for 10 s to fully induce XtTPC3. The current amplitude at each time was normalized by that after induction. The points of injection and induction are indicated by black arrows. The colors of the circles above the plots correspond to those in A. **(C)** Time constants of activation at 100 mV before injection (black; 0 s) and after injection (red; 700 s) for each type of injected PI. **(D)** The normalized amplitudes elicited by 50 mV at 700 s for each type of injected PI. Error bars represent the SD of five independent experiments. *, $P < 0.05$; **, $P < 0.01$.

the phosphate recognition site is changed to TPC1-type, completely abolished induction. Also, the PI injection experiments demonstrated that R53D/N54K lost the PI(3,4)P_2 sensitivity, similar to R187Q (Fig. 12, E and F). These results clearly indicate that the H1-IS0 loop is critical for PI(3,4)P_2 recognition, possibly in terms of PI selectivity.

A structural determinant for the coupling of PI binding with modulation of voltage dependence

Our preceding data suggest that PI(3,4)P_2 binding in XtTPC3 causes the potentiation of voltage dependence, which is hardly observed in the case of the binding of PI(3,5)P_2 to TPC1 (Cang et al., 2014b). Consequently, there should exist a mechanism unique in XtTPC3 for the coupling of the PI binding in domain I with the voltage-dependent gating that is governed by domain II. The XtTPC3 structural model indicates that Arg297 in IS6, which was identified to be important for induction (Fig. 10, D–F), apparently does not participate in the PI binding site, but has an electrostatic interaction with Glu665 in IIS6 (Fig. 13, A and B). In addition to Arg297, the hydroxyl group of Tyr293, which is replaced with phenylalanine in MmTPC1, also interacts with Glu665 with a hydrogen bond. These interactions are likely to

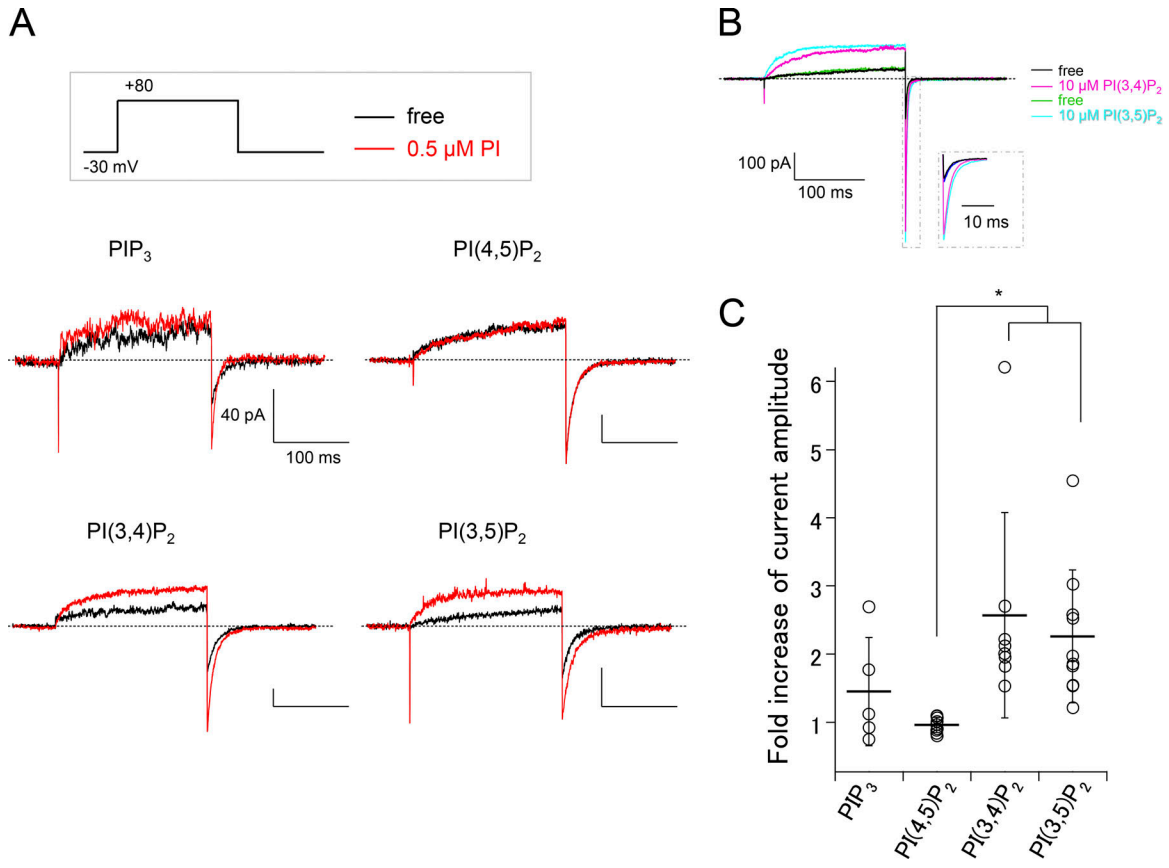

Figure 9. **PI perfusion of inside-out patches expressing XtTPC3. (A)** Representative current recordings before (black) and after (red) PI perfusion in inside-out patches from *Xenopus* oocytes expressing XtTPC3. **(B)** Sequential perfusion of $PI(3,4)P_2$ and $PI(3,5)P_2$ to XtTPC3. Step pulses were given every 10 s. The dotted inset is an expanded view of the tail currents. **(C)** A plot of the fold increase of tail current amplitude by each PI perfusion (0.5 μM) as shown in A. *, $P < 0.05$.

contribute to the induction by coupling the PI-induced IS6 movement to the voltage-dependent IIS6 movement, rather than as the PI binding site itself.

To prove the electrostatic interaction between Arg297 and Glu665, the countercharges were introduced to Arg297 and Glu665 separately and together. R297E attenuated the induction, similar to R297Q (Fig. 13, C–E). Because E665R did not show detectable currents, the neutralizing mutant, E665Q, was alternatively evaluated (Fig. 13 C). Although the current amplitude of E665Q before induction was too small to be analyzed, the G–V relationship after induction showed less extent of induction than WT, similar to R297E (Fig. 13, C–E). In addition, the fatal effect of E665R was rescued by introduction of R297E, producing a charge-swapped double mutation (R297E/E665R), which has a $V_{1/2}$ value after induction comparable to that of WT.

In addition to the electrostatic interaction between Arg297 and Glu665, another contribution of Tyr293 was also evaluated. Unexpectedly, Y293A and even Y293F, which removes only the hydroxyl group, did not produce detectable current (Fig. 13 C). Based on this result, which indicates the critical importance of the polar moiety at the tip of a bulky side chain to form the hydrogen bond with Glu665, the mutations to glutamine and histidine in the 293 position were evaluated. As expected, both Y293Q and Y293H retained the current with the induction property. Although the current before induction of Y293H was too small to be analyzed (Fig. 13 B), the $V_{1/2}$ value after induction showed less change (Fig. 13 C). Y293Q also showed a similar $V_{1/2}$ after induction. These results indicate that the induction requires a bridging interaction of Tyr293, Arg297, and Glu665, which is likely to couple the PI-induced movement of IS6 with the voltage-dependent movement of IIS6.

Discussion

TPC3 is potentiated by $PI(3,4)P_2$ in the plasma membrane

By the addition of the present study, all the members of the TPC family are demonstrated to be PI-sensitive channels, although TPC3 is unique in its $PI(3,4)P_2$ sensitivity. Among the PI species that predominantly localize in the plasma-membrane (PIP_3, $PI(4,5)P_2$, and $PI(3,4)P_2$), XtTPC3 is more clearly potentiated by $PI(3,4)P_2$ and completely insensitive to $PI(4,5)P_2$ (Fig. 8 and Fig. 9). Some inwardly rectifying K^+ channels, such as G protein–coupled inwardly rectifying potassium channel 1/2 (GIRK1/2), GIRK1/4, renal outer medullary potassium channel 1 (ROMK1), and ATP-sensitive potassium channel (K_{ATP}), are known to respond to $PI(3,4)P_2$ to a similar or lesser extent compared with $PI(4,5)P_2$ (Ho

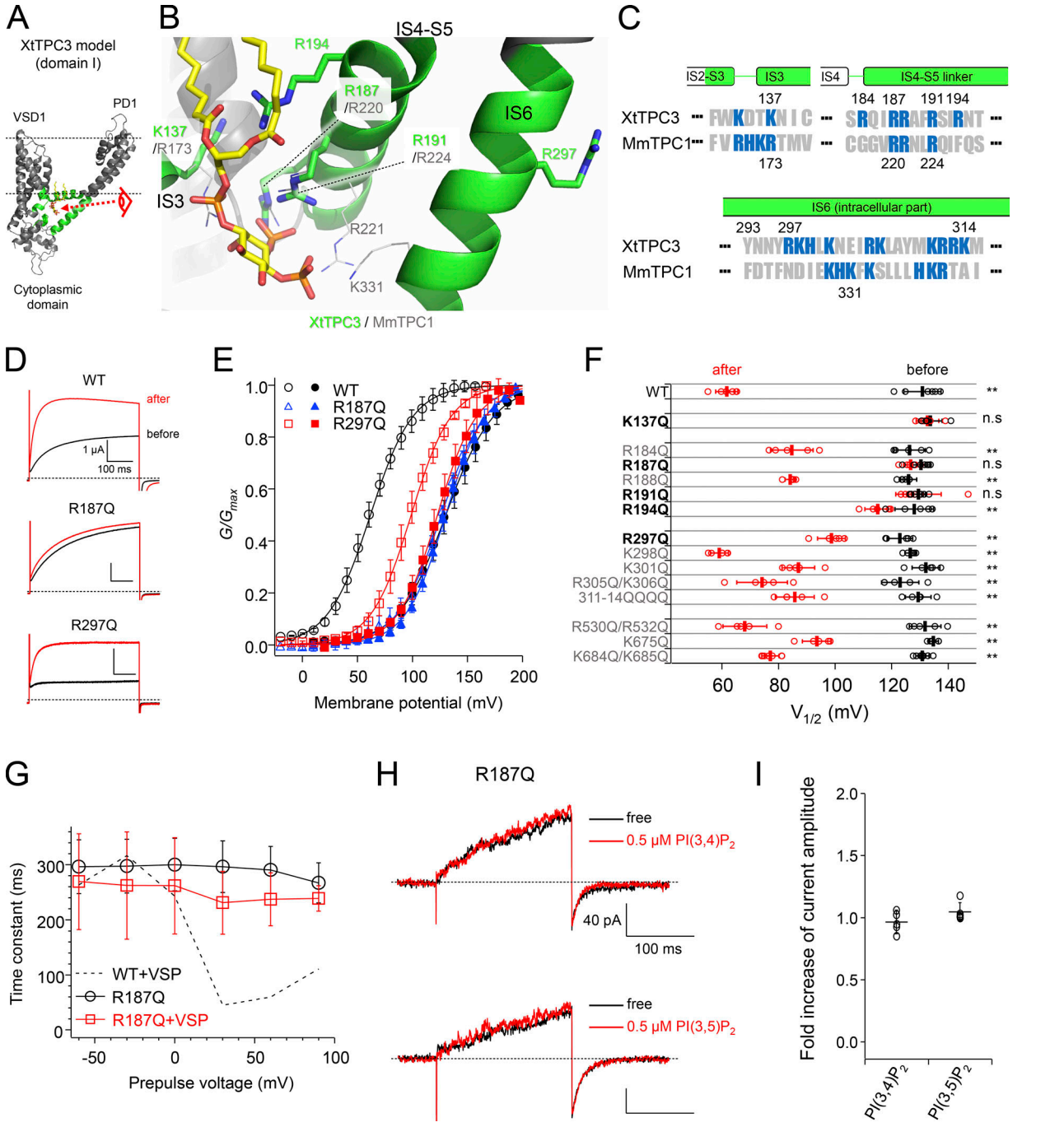

Figure 10. **Identification of the residues critical for both induction and PI(3,4)P_2 recognition. (A)** Overall structure of domain I of the XtTPC3 model. The regions shown in green correspond to those shown in C. The two dotted lines indicate the supposed lipid bilayers. The view from the eye symbol is expanded in B. **(B)** The putative PI binding site in the XtTPC3 model. The MmTPC1 structure (PDB accession no. 6C9A) was superimposed on the XtTPC3 model, and only some side chains and the PI molecule are depicted. **(C)** Sequence alignment of XtTPC3 and MmTPC1. The numbers of the sequences are shown at the top (XtTPC3) and at the bottom (MmTPC1). Basic residues are shown in blue. **(D and E)** Representative traces evoked by a 100-mV test pulse (D) and G–V relationships before (closed) and after (open) induction (E) in WT, R187Q, and R297Q. **(F)** Plots of $V_{1/2}$ in a series of mutants before (black) and after (red) induction. **, $P < 0.05$; n.s., not significant at $P > 0.05$. **(G)** The relationships between time constants of activation and prepulse voltages in R187Q only (black) and coexpressed with Ci-VSP (red). The dotted line indicates the data of WT with Ci-VSP shown in Fig. 4 G. **(H)** Representative current traces from the R187Q mutant in an inside-out patch. Currents were elicited by a +120-mV step pulse from the −30-mV holding potential. **(I)** Fold increase in tail current amplitude by 0.5 μM PI(3,4)P_2 and PI(3,5)P_2 perfusion. Error bars represent the SD of five independent experiments.

and Murrell-Lagnado, 1999; Rohács et al., 1999, 2003; Zeng et al., 2002). Epithelial Na^+ channels are activated by both PI(3,4)P_2 and PIP_3, whose preference is unclear, and requires PI(4,5)P_2 for its basal activity (Tong et al., 2004; Pochynyuk et al., 2007). The activation of TRPML1 by PI(3,5)P_2 is competitively inhibited by PI(3,4)P_2, but also by PI(4,5)P_2 and PIP_3 (Zhang et al., 2012).

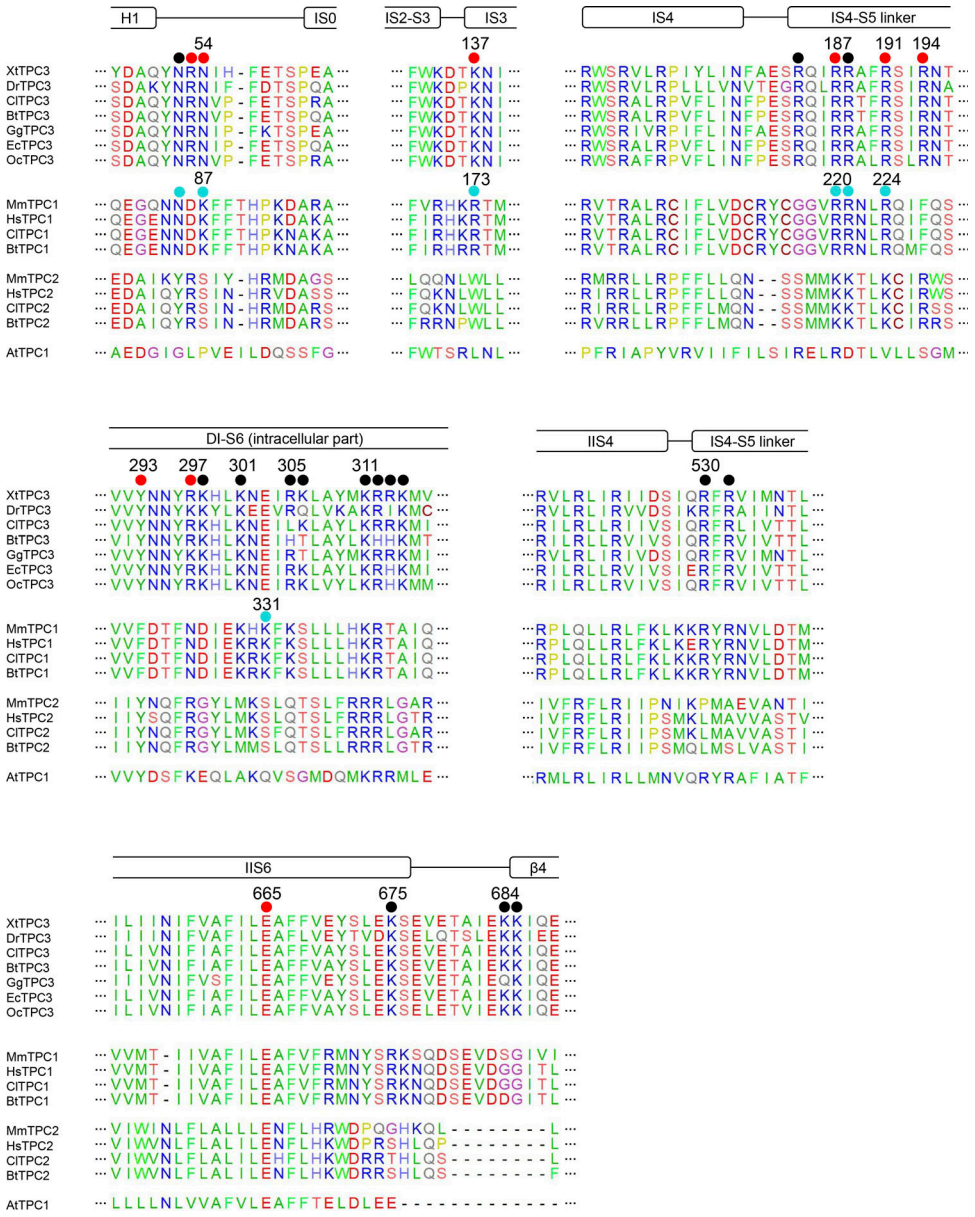

Figure 11. **Alignment of amino acid sequences of TPC1-3 orthologues.** Secondary structures were assigned based on the cryo-EM structure of MmTPC1. The filled circles above the XtTPC sequence indicate the residues that are less important (black) or critical (red) for induction, respectively. The aqua circles above the MmTPC1 sequence indicate the residues that are important for PI(3,5)P_2 recognition. The species of the orthologues are as follows: zebrafish (*D. rerio*, Dr), dog (*Canis lupus*, Cl), cattle (*Bos taurus*, Bt), chicken (*Gallus gallus*, Gg), horse (*Equus caballus*, Ec), rabbit (*Orytolagus cuniculus*, Oc). and *Arabidopsis thaliana* (At).

Therefore, the PI(3,4)P_2 preference of XtTPC3 on the plasma membrane is a unique feature in the PI dependence of ion channels.

The PI perfusion experiment using inside-out patches, a simpler system lacking cytosolic components, clearly showed the PI(3,5)P_2 sensitivity (Fig. 9). The inconsistency of this result with the direct PI injection experiment (Fig. 8) indicates that some mechanisms in the whole oocyte prevent PI(3,5)P_2 action on XtTPC3. PI(3,5)P_2 is known to be selectively accumulated in endosomes and lysosomes, and its localization is strictly regulated by some PI kinases, phosphatases, and binding proteins (Marat and Haucke, 2016). Therefore, the PI(3,5)P_2 injected into *Xenopus* oocytes might be minimally localized in and/or translocated to the plasma membrane. Another possibility is the existence of any mechanism of XtTPC3 and/or cytoplasm to regulate its PI sensitivity. For example, the phosphorylation of TPC3, which could be affected by membrane excision, might regulate its PI sensitivity. Although the issue of the difference in the sensitivity to PI(3,5)P_2 in different conditions remains, the results imply that PI(3,5)P_2 could not behave as a ligand for XtTPC3 expressed in the plasma membrane in whole oocytes.

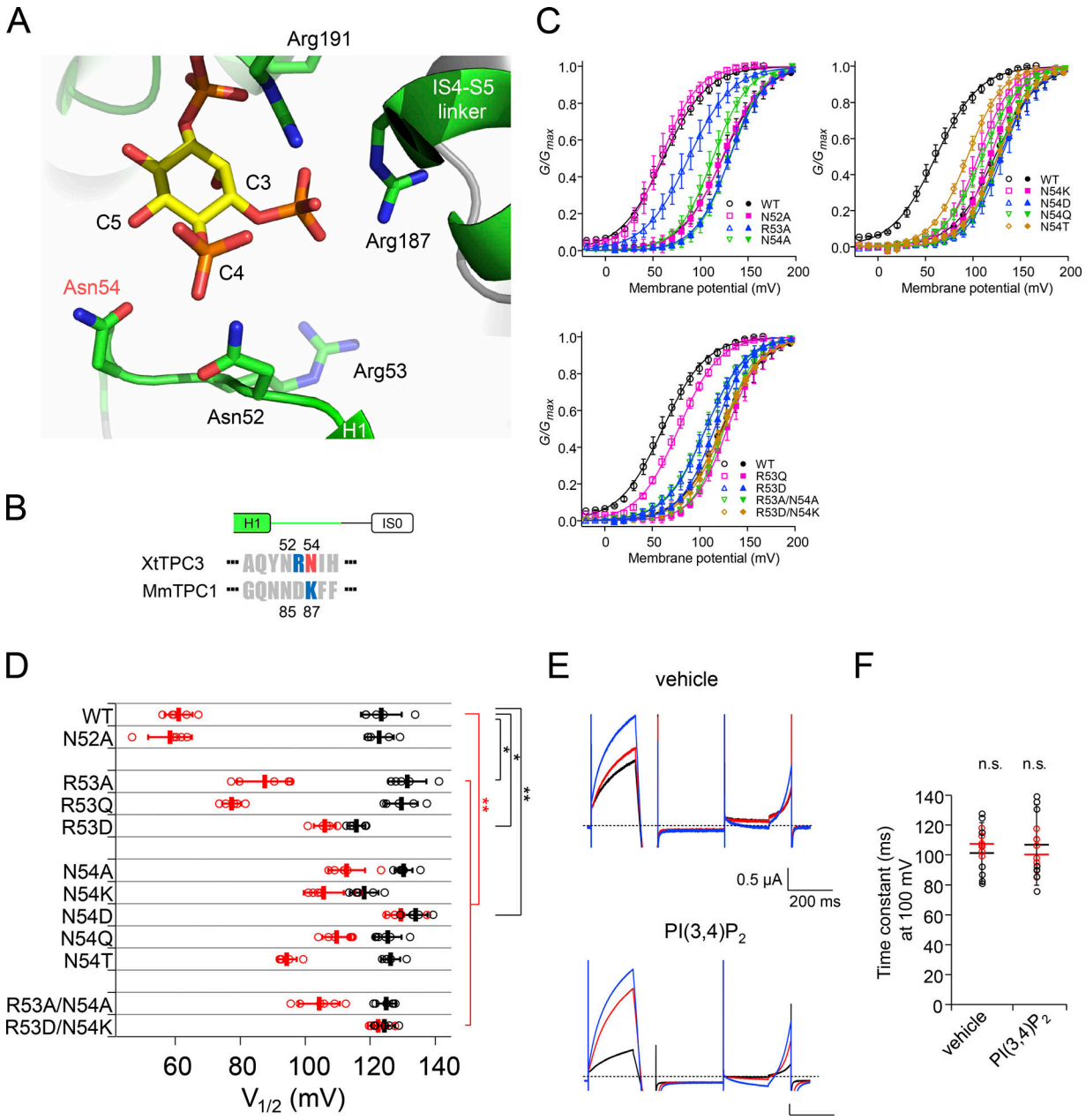

Figure 12. **Effects on induction of mutation of residues in the H1-IS0 loop. (A)** Structural view of the H1-IS0 loop and surrounding region in the XtTPC3 model. **(B)** Sequence alignment of the H1-IS0 loop region in the N-terminal cytoplasmic region of XtTPC3 and MmTPC1. The numbering of the sequences is shown at the top (XtTPC3) and at the bottom (MmTPC1). **(C)** G–V relationships of XtTPC3 with mutations at Asn52, Arg53, and Asn54. **(D)** Plots of $V_{1/2}$ in a series of mutants before (black) and after (red) induction. **(E)** Representative current traces of R53D/N54K in oocytes injected with vehicle and $PI(3,4)P_2$. In each case, the traces before injection (black), after injection (red), and after induction (blue) were obtained by the same protocol as shown in Fig. 8 A. **(F)** Time constants of activation at 100 mV before (black) and after (red) injection are shown for each type of injected PI. Error bars represent the SD of five to seven independent experiments. n.s., not significant at $P > 0.05$; *, $P < 0.05$; **, < 0.01.

A previous work reported that TPC3 from *D. rerio* expressed in endolysosomal membranes is insensitive to $PI(3,5)P_2$ (Cang et al., 2014a). This is in remarkable contrast with our inside-out patch experiments (Fig. 9). We think it is due to low luminal pH in their experimental condition, since we newly found that low extracellular (i.e., luminal) pH (pH 4.6) significantly inhibited the "induced" (PI-bound) XtTPC3 (Fig. 14). Therefore, TPC3 in endosomes and lysosomes cannot be highly activated due to their low luminal pH (Xu and Ren, 2015), despite the enriched $PI(3,5)P_2$ there. These notions indicate that the actual physiological ligand and functioning location for TPC3 is $PI(3,4)P_2$ and the plasma membrane, rather than $PI(3,5)P_2$ and endosomes and lysosomes.

A model for $PI(3,4)P_2$ sensitivity

The residues important for PI recognition in XtTPC3 are quite similar to those for $PI(3,5)P_2$ in TPC1, although there are some differences, which could explain the $PI(3,4)P_2$ sensitivity of

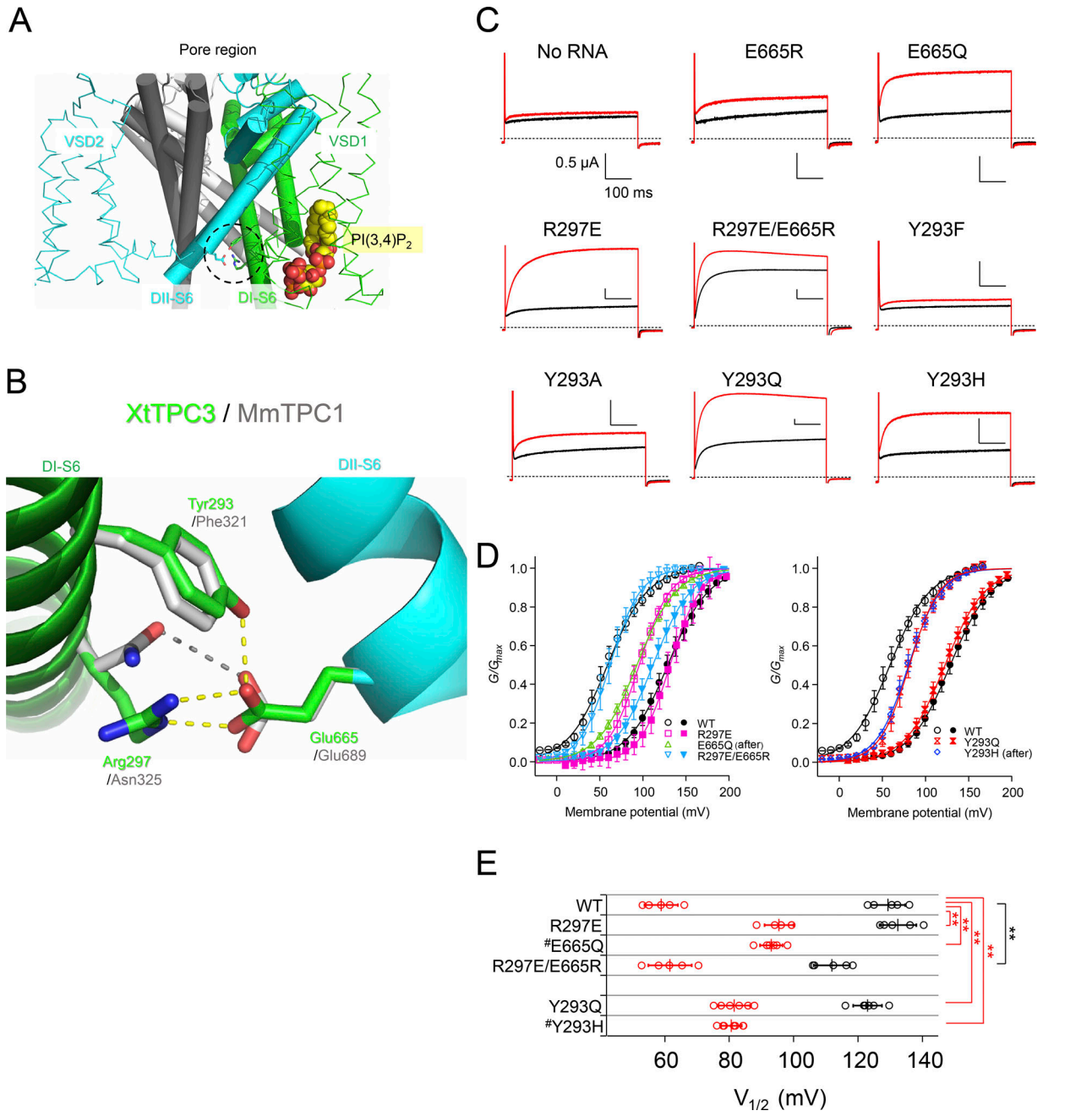

Figure 13. **Critical importance of the interaction between IS6 and IIS6 to induction. (A)** A view of the XtTPC3 structural model in the PI(3,4)P_2-bound open state, depicting the regions related to PI(3,4)P_2 binding and coupling with voltage dependence. Domain I and domain II in one monomer are depicted in green and aqua, respectively. Those in the other monomer are shown in white and gray, and the VSDs are omitted for clarity. VSDs and pore domains are shown as ribbon and cylinder models, respectively. The region indicated by the dotted circle shows the interaction that bridges the DI-S6 and DII-S6 (Tyr293, Arg297, and Glu665). **(B)** Structural view of the proximal region between the cytosolic parts of IS6 and IIS6 in the superimposed structures of XtTPC3 and MmTPC1. The carbon atoms of side chains are shown in green for XtTPC3 and in white for MmTPC1. Dashed lines indicate putative hydrogen bonds with distances of 2.6–3.3 Å in the model structures. **(C)** Representative current traces of a series of channels with mutations at Tyr293, Arg297, and Glu665 before (black) and after (red) induction. Currents were evoked by a 100-mV pulse from −60 mV. **(D)** G–V relationships of channels with mutations at Tyr293, Arg297, or Glu665. **(E)** Plots of $V_{1/2}$ in a series of mutants of Tyr293, Arg297, and Glu665 before (black) and after (red) induction. #, the $V_{1/2}$ values before induction in E665Q and Y293H could not be obtained because the currents were too small. Error bars represent the SD of five to seven independent experiments. **, P < 0.01.

XtTPC3 (Fig. 10, B–F). In the MmTPC1 structure, three arginines in the IS4-S5 linker form salt bridges with the C3 phosphate of PI(3,5)P_2 and hence contribute to the exclusion of PIs lacking C3 phosphate, such as PI(4,5)P_2. XtTPC3 retains the corresponding arginines, two of which are important for induction (Arg187 and Arg 191), but the other one (Arg188) is apparently less critical (Fig. 10 F). Alternatively, Arg194, which is not conserved in TPC1, is critically important. The XtTPC3 homology model

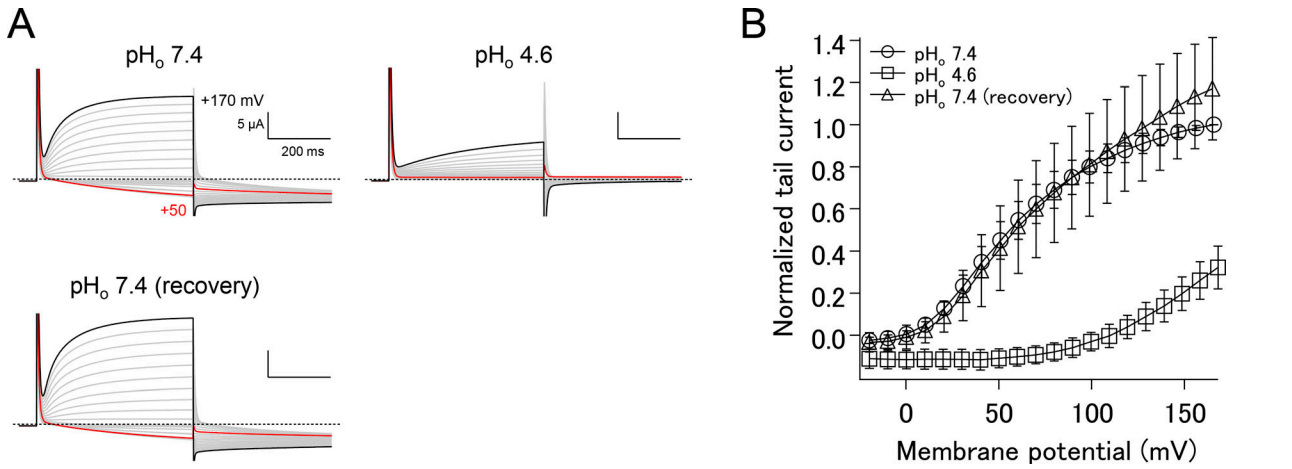

Figure 14. **Extracellular pH dependent change of XtTPC3 current in the whole cell configuration. (A)** Representative current recordings from *Xenopus* oocytes expressing XtTPC3 by two-electrode voltage clamp in extracellular pH (pH$_o$) 7.4 (left, top), in pH$_o$ 4.6 (right, top) and upon return to pH$_o$ 7.4 (left, bottom). Currents were elicited from −60-mV holding potential to various step pulses in the same protocol to obtain the G–V relationships after induction as shown in Fig. 1 C, right. **(B)** Plots of the tail current amplitude normalized to that before pH change. Error bars represent the SD of five independent experiments.

indicates that Arg187 and Arg191 interact with the C3 phosphate, similar to MmTPC1, and that Arg194 is located close to the carbonyl oxygens of acyl chains (Fig. 10 B). The model also shows that the side chain of Arg194 would collide sterically with the PI molecule. Therefore, to accommodate the acyl chains near Arg194, the PI molecule might be pushed and rotated from the original position, but the extensive salt bridges for C3 phosphate imply that the C3 position could be maintained. This repositioning might direct the C4 and C5 positions to the appropriate location to interact with residues in the H1-IS0 loop region, and therefore, the precise PI position has to be modified from our original model (Fig. 10 B and Fig. 12 A).

To recognize PI(3,4)P_2, Asn54 in the H1-IS0 region is thought to be critical (Fig. 12). The large effects on induction by a slight change of the side chain, such as elongation (glutamine) and a negative charge with the same size (aspartate), indicate the asparagine residue here is needed to exactly recognize PI(3,4)P_2. The intolerance of positively charged lysine and the mild effect of the substitution of polar threonine suggest that Asn54 does not interact with the negatively charged phosphate groups, but is likely to form a hydrogen bond with the polar part of PI(3,4)P_2 (Fig. 12, C and D). In the XtTPC3 model, Asn54 is located nearest to the C5 hydroxyl group of the PI(3,4)P_2 molecule, although they are located a little too distant from each other to form a hydrogen bond. This positional relationship is similar to the model for PI(3,5)P_2 discrimination in MmTPC1, where the amino group of Asn85 interacts with the C4 hydroxyl group but would sterically hinder binding in the presence of a C4 phosphate group (She et al., 2018). The repositioning, caused by the interaction with Arg194 as mentioned in the previous paragraph, may move the C5 hydroxyl group of PI(3,4)P_2 closer to Asn54, to form a hydrogen bond. PI(3,5)P_2 might somehow bind to XtTPC3 by the contribution of Asn52, whose corresponding residue in MmTPC1 is important for PI(3,5)P_2 binding. This model could be verified by further structural studies of TPC3.

A mechanism for PI-dependent modulation of the voltage dependence

Strong PI-dependent modulation of the voltage dependence is another special feature of TPC3. It is presumably achieved by two mechanisms, namely PI-induced IS6 movement, which is thought to be similar among TPCs, and a tight coupling of IS6 with IIS6. Based on the cryo-EM structures of MmTPC1 with or without PI(3,5)P_2, PI binding induces a conformational rearrangement in the H1-IS0 loop, the cytosolic part of VSD1, and the linker region between domain I/II, and finally, leads to IS6 movement to expand the activation gate (Fig. S6). In MmTPC1, although the PI binding increases macroscopic current amplitudes, it induces only a slight or no shift of voltage dependence (Cang et al., 2014b; She et al., 2018). This indicates that PI-induced IS6 movement and voltage-dependent IIS6 movement are relatively independent in TPC1. In the case of TPC3, the interaction between Tyr293 and Arg297 in IS6 and Glu665 in IIS6 is expected to strengthen the IS6–IIS6 coupling (Fig. 13 B). Because the disruption of this interaction, such as in R297Q, R297E, and Y293Q, showed no profound effects on the $V_{1/2}$ before induction (Fig. 10 F and Fig. 13 E), the interaction is likely to be formed in the PI(3,4)P_2-bound state (Fig. 15). The tight interaction between IS6 and IIS6 could transmit the conformational change of IS6 induced by PI(3,4)P_2 binding to IIS6 to facilitate its movement for gate opening (Fig. 15). As less energy is required to direct IIS6 toward its opening conformation thanks to PI(3,4)P_2-bound IS6, VSD2 needs less voltage stimulus to open the gate. This could be the cause of the negative shift of the G–V relationship after induction.

As Glu665 in IIS6 is conserved and the position for Arg297 in IS6 is replaced with asparagine in TPC1 orthologues (Fig. 11), the weak interaction using a hydrogen bond between glutamate and asparagine might be evolutionally conserved between IS6 and IIS6 in TPC1s. The necessity of, at least, the minimum interaction might reflect the indispensable linking between IS6 and IIS6 for channel gating, regardless of the presence or absence of

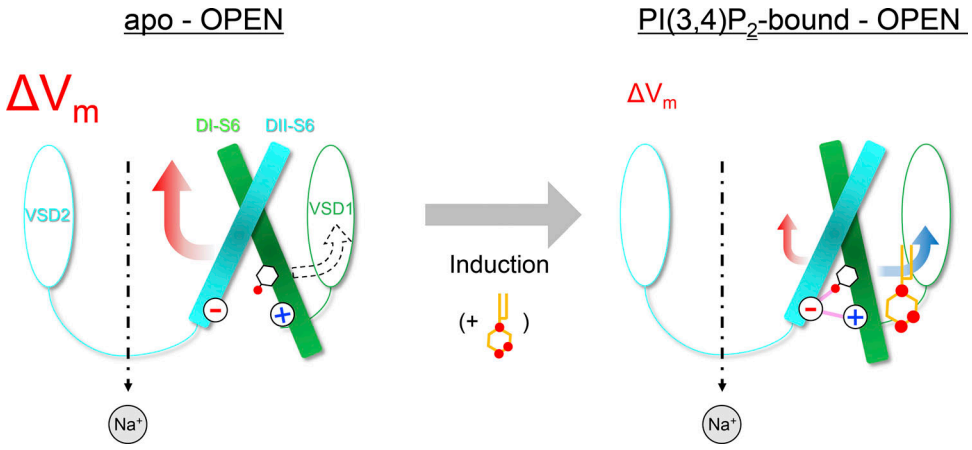

Figure 15. **A structural model for induction, PI(3,4)P_2-induced modulation of voltage dependence.** The induction model. The model depiction is based on the structure shown in Fig. 13 A. In the apo-state, or before induction (left), a strong voltage stimulus (red arrow) is required to direct both DI-S6 and DII-S6, which are thought to be weakly linked, to the open conformation. In the PI(3,4)P_2-bound state, or after induction (right), PI(3,4)P_2 binding facilitates the opening of the activation gate through the tight interaction between DI-S6 and DII-S6, which is formed in this state. As some of the required energy to move both S6s is provided by PI(3,4)P_2 binding (blue arrow), less voltage stimulus is required to open the activation gate than in the case of the apo state. V_m indicates membrane voltage.

PI-dependent modulation of the voltage dependence. In XtTPC3, a strong interaction is formed by a salt bridge and supported further by the hydroxyl group of Tyr293 (Fig. 13 B). Notably, Arg297 and Tyr 293 are also conserved among TPC3 orthologues (Fig. 11). These observations suggest that, in each TPC family, the extent of mutual dependence between PIs and voltage is optimized through the IS6–IIS6 interactions. The weak interaction between IS6 and IIS6 means that TPC1 opens only when both voltage and PI are sufficiently applied, while the tight interaction in TPC3 could integrate the two stimuli, where one stronger stimulus might compensate for the other weaker stimulus (Fig. 15). Interestingly, the tyrosine and the basic residues in IS6 are also conserved in the TPC2 family, as well as in TPC1 from *A. thaliana* (AtTPC1), which is gated by voltage and Ca^{2+} (Fig. 11; Guo et al., 2016; Kintzer and Stroud, 2016). Because TPC2 is a PI-dependent and non–voltage-dependent channel (Wang et al., 2012), PI binding needs to provide the energy sufficient to open the gate without any contribution from VSDs. Very recently solved cryo-EM structures of human TPC2 in the apo- and PI(3,5)P_2-bound states reveal that the distance between those residues decreases in the PI(3,5)P_2-bound state (She et al., 2019). The tight IS6–IIS6 interaction identified in this study might contribute to enabling movement of both IS6 and IIS6, so that gate opening in TPC2 occurs in response to PI binding alone. In AtTPC1, Ca^{2+} binding to the linker region between domains I and II, which is located just beneath IS6, is known to modulate the voltage dependence (Guo et al., 2016). Therefore, similarly to XtTPC3, Ca^{2+}-induced IS6 movement might affect the voltage-dependent IIS6 movement through the IS6–IIS6 interaction in AtTPC1.

Implication for physiological roles of TPC3 and PI(3,4)P_2 in *Xenopus* oocyte

The PI(3,4)P_2-dependent modulation is thought to be evolutionally conserved among TPC3 orthologues, because the basic residues important for induction are almost completely conserved among most TPC3 orthologues (Fig. 11). TPC3 mRNA or protein is reported to exist in oocytes of sea urchin (Ruas et al., 2010; Patel et al., 2011) and *X. laevis* (Cang et al., 2014a), and known to play a role in fertilization and development in starfish oocytes (Ramos et al., 2014). Some eggs, including those of *Xenopus*, show a long-lasting depolarization, the so-called fertilization potential (Cross and Elinson, 1980; Grey et al., 1982), that is induced by sperm entry and causes polyspermy block. Interestingly, in *X. laevis*, Na^+ conductance is reported to transiently appear during the fertilization potential in eggs (Peres and Mancinelli, 1985) or by applying a long depolarization in oocytes (Baud et al., 1982). In addition, the PI3K activity that produces PI(3,4)P_2 is known to increase before fertilization, during the maturation step, in *Xenopus* oocytes (Liu et al., 1995; Hehl et al., 2001). Taking these data into consideration, TPC3 is likely to be activated at fertilization, as both depolarization voltage and PI(3,4)P_2 stimuli are provided, and to contribute to the fertilization potential through its Na^+ permeability. These data suggest a contribution of PI(3,4)P_2 to oocyte fertilization through TPC3.

Data availability

All the data sets generated for this study are available from the corresponding author in response to reasonable requests.

Acknowledgments

We thank Dr. Y. Fujiyoshi (Nagoya University, Nagoya, Japan) for kindly providing us with the XtTPC3 cDNA, Dr Y. Okamura (Osaka University, Osaka, Japan) for the Ci-VSP cDNA, and Dr. E.Y. Isacoff (University of California, Berkeley, Berkeley, CA) for F-TAPP and F-PLC cDNAs. We also thank Ms. C. Naito for technical support, and all the members of the Kubo laboratory for valuable discussion. We thank Dr. A. Collins (Saba University

School of Medicine, Dutch Caribbean) for editing and refining the manuscript.

This work was supported by the Grant-in-Aid for Young Scientists (18K15019 to T. Shimomura) and the Scientific Research (B) (17H04021 to Y. Kubo) from the Japan Society for the Promotion of Science.

The authors declare no competing financial interests.

Author contributions: T. Shimomura conceived the study with Y. Kubo and designed the experiments. T. Shimomura performed all experiments and data analyses. T. Shimomura wrote the initial draft, and T. Shimomura and Y. Kubo completed the manuscript. Both authors have approved the final version of the manuscript.

Merritt C. Maduke served as editor.

Submitted: 31 October 2018
Revised: 26 April 2019
Accepted: 23 May 2019

References

Aggarwal, S.K., and R. MacKinnon. 1996. Contribution of the S4 segment to gating charge in the Shaker K+ channel. *Neuron.* 16:1169–1177. https://doi.org/10.1016/S0896-6273(00)80143-9

Armstrong, C.M., F. Bezanilla, and W. Hole. 1974. Charge movement associated with the opening and closing of the activation gates of the Na channels. *J. Gen. Physiol.* 63:533–552. https://doi.org/10.1085/jgp.63.5.533

Bae, Y.H., Z. Ding, T. Das, A. Wells, F. Gertler, and P. Roy. 2010. Profilin1 regulates PI(3,4)P2 and lamellipodin accumulation at the leading edge thus influencing motility of MDA-MB-231 cells. *Proc. Natl. Acad. Sci. USA.* 107:21547–21552. https://doi.org/10.1073/pnas.1002309107

Balla, T. 2013. Phosphoinositides: tiny lipids with giant impact on cell regulation. *Physiol. Rev.* 93:1019–1137. https://doi.org/10.1152/physrev.00028.2012

Barish, M.E. 1983. A transient calcium-dependent chloride current in the immature Xenopus oocyte. *J. Physiol.* 342:309–325. https://doi.org/10.1113/jphysiol.1983.sp014852

Baud, C., R.T. Kado, and K. Marcher. 1982. Sodium channels induced by depolarization of the Xenopus laevis oocyte. *Proc. Natl. Acad. Sci. USA.* 79:3188–3192. https://doi.org/10.1073/pnas.79.10.3188

Boucrot, E., A.P.A. Ferreira, L. Almeida-Souza, S. Debard, Y. Vallis, G. Howard, L. Bertot, N. Sauvonnet, and H.T. McMahon. 2015. Endophilin marks and controls a clathrin-independent endocytic pathway. *Nature.* 517:460–465. https://doi.org/10.1038/nature14067

Braccini, L., E. Ciraolo, C.C. Campa, A. Perino, D.L. Longo, G. Tibolla, M. Pregnolato, Y. Cao, B. Tassone, F. Damilano, et al. 2015. PI3K-C2γ is a Rab5 effector selectively controlling endosomal Akt2 activation downstream of insulin signalling. *Nat. Commun.* 6:7400. https://doi.org/10.1038/ncomms8400

Brailoiu, E., D. Churamani, X. Cai, M.G. Schrlau, G.C. Brailoiu, X. Gao, R. Hooper, M.J. Boulware, N.J. Dun, J.S. Marchant, and S. Patel. 2009. Essential requirement for two-pore channel 1 in NAADP-mediated calcium signaling. *J. Cell Biol.* 186:201–209. https://doi.org/10.1083/jcb.200904073

Brailoiu, E., R. Hooper, X. Cai, G.C. Brailoiu, M.V. Keebler, N.J. Dun, J.S. Marchant, and S. Patel. 2010. An ancestral deuterostome family of two-pore channels mediates nicotinic acid adenine dinucleotide phosphate-dependent calcium release from acidic organelles. *J. Biol. Chem.* 285:2897–2901. https://doi.org/10.1074/jbc.C109.081943

Cai, X., and S. Patel. 2010. Degeneration of an intracellular ion channel in the primate lineage by relaxation of selective constraints. *Mol. Biol. Evol.* 27:2352–2359. https://doi.org/10.1093/molbev/msq122

Calcraft, P.J., M. Ruas, Z. Pan, X. Cheng, A. Arredouani, X. Hao, J. Tang, K. Rietdorf, L. Teboul, K.T. Chuang, et al. 2009. NAADP mobilizes calcium from acidic organelles through two-pore channels. *Nature.* 459:596–600. https://doi.org/10.1038/nature08030

Cang, C., Y. Zhou, B. Navarro, Y.J. Seo, K. Aranda, L. Shi, S. Battaglia-Hsu, I. Nissim, D.E. Clapham, and D. Ren. 2013. mTOR regulates lysosomal ATP-sensitive two-pore Na(+) channels to adapt to metabolic state. *Cell.* 152:778–790. https://doi.org/10.1016/j.cell.2013.01.023

Cang, C., K. Aranda, and D. Ren. 2014a. A non-inactivating high-voltage-activated two-pore Na^+ channel that supports ultra-long action potentials and membrane bistability. *Nat. Commun.* 5:5015. https://doi.org/10.1038/ncomms6015

Cang, C., B. Bekele, and D. Ren. 2014b. The voltage-gated sodium channel TPC1 confers endolysosomal excitability. *Nat. Chem. Biol.* 10:463–469. https://doi.org/10.1038/nchembio.1522

Cross, N.L., and R.P. Elinson. 1980. A fast block to polyspermy in frogs mediated by changes in the membrane potential. *Dev. Biol.* 75:187–198. https://doi.org/10.1016/0012-1606(80)90154-2

Dong, X.P., D. Shen, X. Wang, T. Dawson, X. Li, Q. Zhang, X. Cheng, Y. Zhang, L.S. Weisman, M. Delling, and H. Xu. 2010. PI(3,5)P(2) controls membrane trafficking by direct activation of mucolipin Ca(2+) release channels in the endolysosome. *Nat. Commun.* 1:38. https://doi.org/10.1038/ncomms1037

García-Rúa, V., S. Feijóo-Bandín, D. Rodríguez-Penas, A. Mosquera-Leal, E. Abu-Assi, A. Beiras, L. María Seoane, P. Lear, J. Parrington, M. Portolés, et al. 2016. Endolysosomal two-pore channels regulate autophagy in cardiomyocytes. *J. Physiol.* 594:3061–3077. https://doi.org/10.1113/JP271332

Grey, R.D., M.J. Bastiani, D.J. Webb, and E.R. Schertel. 1982. An electrical block is required to prevent polyspermy in eggs fertilized by natural mating of Xenopus laevis. *Dev. Biol.* 89:475–484. https://doi.org/10.1016/0012-1606(82)90335-9

Grimm, S.S., and E.Y. Isacoff. 2016. Allosteric substrate switching in a voltage-sensing lipid phosphatase. *Nat. Chem. Biol.* 12:261–267. https://doi.org/10.1038/nchembio.2022

Guo, J., W. Zeng, Q. Chen, C. Lee, L. Chen, Y. Yang, C. Cang, D. Ren, and Y. Jiang. 2016. Structure of the voltage-gated two-pore channel TPC1 from Arabidopsis thaliana. *Nature.* 531:196–201. https://doi.org/10.1038/nature16446

Hehl, S., B. Stoyanov, W. Oehrl, R. Schönherr, R. Wetzker, and S.H. Heinemann. 2001. Phosphoinositide 3-kinase-gamma induces Xenopus oocyte maturation via lipid kinase activity. *Biochem. J.* 360:691–698. https://doi.org/10.1042/bj3600691

Ho, I.H.M., and R.D. Murrell-Lagnado. 1999. Molecular mechanism for sodium-dependent activation of G protein-gated K+ channels. *J. Physiol.* 520:645–651. https://doi.org/10.1111/j.1469-7793.1999.00645.x

Hogan, A., Y. Yakubchyk, J. Chabot, C. Obagi, E. Daher, K. Maekawa, and S.H. Gee. 2004. The phosphoinositol 3,4-bisphosphate-binding protein TAPP1 interacts with syntrophins and regulates actin cytoskeletal organization. *J. Biol. Chem.* 279:53717–53724. https://doi.org/10.1074/jbc.M410654200

Kintzer, A.F., and R.M. Stroud. 2016. Structure, inhibition and regulation of two-pore channel TPC1 from Arabidopsis thaliana. *Nature.* 531:258–262. https://doi.org/10.1038/nature17194

Kume, S., T. Shimomura, M. Tateyama, and Y. Kubo. 2018. Two mutations at different positions in the CNBH domain of the hERG channel accelerate deactivation and impair the interaction with the EAG domain. *J. Physiol.* 596:4629–4650. https://doi.org/10.1113/JP276208

Kurokawa, T., S. Takasuga, S. Sakata, S. Yamaguchi, S. Horie, K.J. Homma, T. Sasaki, and Y. Okamura. 2012. 3′ Phosphatase activity toward phosphatidylinositol 3,4-bisphosphate [PI(3,4)P2] by voltage-sensing phosphatase (VSP). *Proc. Natl. Acad. Sci. USA.* 109:10089–10094. https://doi.org/10.1073/pnas.1203799109

Li, H., and A.J. Marshall. 2015. Phosphatidylinositol (3,4) bisphosphate-specific phosphatases and effector proteins: A distinct branch of PI3K signaling. *Cell. Signal.* 27:1789–1798. https://doi.org/10.1016/j.cellsig.2015.05.013

Li, H., X. Wu, S. Hou, M. Malek, A. Kielkowska, E. Noh, K.J. Makondo, Q. Du, J.A. Wilkins, J.B. Johnston, et al. 2016. Phosphatidylinositol-3,4-Bisphosphate and Its Binding Protein Lamellipodin Regulate Chemotaxis of Malignant B Lymphocytes. *J. Immunol.* 196:586–595. https://doi.org/10.4049/jimmunol.1500630

Lin, P.-H., P. Duann, S. Komazaki, K.H. Park, H. Li, M. Sun, M. Sermersheim, K. Gumpper, J. Parrington, A. Galione, et al. 2015. Lysosomal two-pore channel subtype 2 (TPC2) regulates skeletal muscle autophagic signaling. *J. Biol. Chem.* 290:3377–3389. https://doi.org/10.1074/jbc.M114.608471

Liu, X.J., A. Sorisky, L. Zhu, and T. Pawson. 1995. Molecular cloning of an amphibian insulin receptor substrate 1-like cDNA and involvement of

phosphatidylinositol 3-kinase in insulin-induced Xenopus oocyte maturation. *Mol. Cell. Biol.* 15:3563–3570. https://doi.org/10.1128/MCB.15.7.3563

Manning, B.D., and A. Toker. 2017. AKT/PKB Signaling: Navigating the Network. *Cell.* 169:381–405. https://doi.org/10.1016/j.cell.2017.04.001

Marat, A.L., and V. Haucke. 2016. Phosphatidylinositol 3-phosphates-at the interface between cell signalling and membrane traffic. *EMBO J.* 35: 561–579. https://doi.org/10.15252/embj.201593564

Murata, Y., H. Iwasaki, M. Sasaki, K. Inaba, and Y. Okamura. 2005. Phosphoinositide phosphatase activity coupled to an intrinsic voltage sensor. *Nature.* 435:1239–1243. https://doi.org/10.1038/nature03650

Patel, S., L. Ramakrishnan, T. Rahman, A. Hamdoun, J.S. Marchant, C.W. Taylor, and E. Brailoiu. 2011. The endo-lysosomal system as an NAADP-sensitive acidic Ca(2+) store: role for the two-pore channels. *Cell Calcium.* 50:157–167. https://doi.org/10.1016/j.ceca.2011.03.011

Patel, S., D. Churamani, and E. Brailoiu. 2017. NAADP-evoked Ca^{2+} signals through two-pore channel-1 require arginine residues in the first S4-S5 linker. *Cell Calcium.* 68:1–4. https://doi.org/10.1016/j.ceca.2017.09.003

Peiter, E., F.J.M. Maathuis, L.N. Mills, H. Knight, J. Pelloux, A.M. Hetherington, and D. Sanders. 2005. The vacuolar Ca2+-activated channel TPC1 regulates germination and stomatal movement. *Nature.* 434: 404–408. https://doi.org/10.1038/nature03381

Peres, A., and E. Mancinelli. 1985. Sodium conductance and the activation potential in Xenopus laevis eggs. *Pflugers Arch.* 405:29–36. https://doi.org/10.1007/BF00591094

Pochynyuk, O., Q. Tong, J. Medina, A. Vandewalle, A. Staruschenko, V. Bugaj, and J.D. Stockand. 2007. Molecular determinants of $PI(4,5)P_2$ and $PI(3,4,5)P_3$ regulation of the epithelial Na^+ channel. *J. Gen. Physiol.* 130: 399–413. https://doi.org/10.1085/jgp.200709800

Posor, Y., M. Eichhorn-Gruenig, D. Puchkov, J. Schöneberg, A. Ullrich, A. Lampe, R. Müller, S. Zarbakhsh, F. Gulluni, E. Hirsch, et al. 2013. Spatiotemporal control of endocytosis by phosphatidylinositol-3,4-bisphosphate. *Nature.* 499:233–237. https://doi.org/10.1038/nature12360

Ramos, I., A. Reich, and G.M. Wessel. 2014. Two-pore channels function in calcium regulation in sea star oocytes and embryos. *Development.* 141: 4598–4609. https://doi.org/10.1242/dev.113563

Ratzan, W.J., A.V. Evsikov, Y. Okamura, and L.A. Jaffe. 2011. Voltage sensitive phosphoinositide phosphatases of Xenopus: their tissue distribution and voltage dependence. *J. Cell. Physiol.* 226:2740–2746. https://doi.org/10.1002/jcp.22854

Rohács, T., J. Chen, G.D. Prestwich, and D.E. Logothetis. 1999. Distinct specificities of inwardly rectifying K(+) channels for phosphoinositides. *J. Biol. Chem.* 274:36065–36072. https://doi.org/10.1074/jbc.274.51.36065

Rohács, T., C.M.B. Lopes, T. Jin, P.P. Ramdya, Z. Molnár, and D.E. Logothetis. 2003. Specificity of activation by phosphoinositides determines lipid regulation of Kir channels. *Proc. Natl. Acad. Sci. USA.* 100:745–750. https://doi.org/10.1073/pnas.0236364100

Ruas, M., K. Rietdorf, A. Arredouani, L.C. Davis, E. Lloyd-Evans, H. Koegel, T.M. Funnell, A.J. Morgan, J.A. Ward, K. Watanabe, et al. 2010. Purified TPC isoforms form NAADP receptors with distinct roles for Ca(2+) signaling and endolysosomal trafficking. *Curr. Biol.* 20:703–709. https://doi.org/10.1016/j.cub.2010.02.049

Sakurai, Y., A.A. Kolokoltsov, C.-C. Chen, M.W. Tidwell, W.E. Bauta, N. Klugbauer, C. Grimm, C. Wahl-Schott, M. Biel, and R.A. Davey. 2015. Ebola virus. Two-pore channels control Ebola virus host cell entry and are drug targets for disease treatment. *Science.* 347:995–998. https://doi.org/10.1126/science.1258758

Sasaki, J., S. Kofuji, R. Itoh, T. Momiyama, K. Takayama, H. Murakami, S. Chida, Y. Tsuya, S. Takasuga, S. Eguchi, et al. 2010. The PtdIns(3,4)P(2) phosphatase INPP4A is a suppressor of excitotoxic neuronal death. *Nature.* 465:497–501. https://doi.org/10.1038/nature09023

Schwede, T., J. Kopp, N. Guex, and M.C. Peitsch. 2003. SWISS-MODEL: An automated protein homology-modeling server. *Nucleic Acids Res.* 31: 3381–3385. https://doi.org/10.1093/nar/gkg520

Seoh, S.A., D. Sigg, D.M. Papazian, and F. Bezanilla. 1996. Voltage-sensing residues in the S2 and S4 segments of the Shaker K+ channel. *Neuron.* 16:1159–1167. https://doi.org/10.1016/S0896-6273(00)80142-7

She, J., J. Guo, Q. Chen, W. Zeng, Y. Jiang, and X.C. Bai. 2018. Structural insights into the voltage and phospholipid activation of the mammalian TPC1 channel. *Nature.* 556:130–134. https://doi.org/10.1038/nature26139

She, J., W. Zeng, J. Guo, Q. Chen, X.C. Bai, and Y. Jiang. 2019. Structural mechanisms of phospholipid activation of the human TPC2 channel. *eLife.* 8:e45222. https://doi.org/10.7554/eLife.45222

Tong, Q., N. Gamper, J.L. Medina, M.S. Shapiro, and J.D. Stockand. 2004. Direct activation of the epithelial Na(+) channel by phosphatidylinositol 3,4,5-trisphosphate and phosphatidylinositol 3,4-bisphosphate produced by phosphoinositide 3-OH kinase. *J. Biol. Chem.* 279:22654–22663. https://doi.org/10.1074/jbc.M401004200

Wang, X., X. Zhang, X.P. Dong, M. Samie, X. Li, X. Cheng, A. Goschka, D. Shen, Y. Zhou, J. Harlow, et al. 2012. TPC proteins are phosphoinositide-activated sodium-selective ion channels in endosomes and lysosomes. *Cell.* 151:372–383. https://doi.org/10.1016/j.cell.2012.08.036

Xu, H., and D. Ren. 2015. Lysosomal physiology. *Annu. Rev. Physiol.* 77:57–80. https://doi.org/10.1146/annurev-physiol-021014-071649

Yu, F.H., and W.A. Catterall. 2004. The VGL-chanome: a protein superfamily specialized for electrical signaling and ionic homeostasis. *Sci. STKE.* 2004:re15. https://doi.org/10.1126/stke.2532004re15

Zeng, W.-Z., H.-H. Liou, U.M. Krishna, J.R. Falck, and C.-L. Huang. 2002. Structural determinants and specificities for ROMK1-phosphoinositide interaction. *Am. J. Physiol. Renal Physiol.* 282:F826–F834. https://doi.org/10.1152/ajprenal.00300.2001

Zhang, X., X. Chen, C. Jia, X. Geng, X. Du, and H. Zhang. 2010. Depolarization increases phosphatidylinositol (PI) 4,5-bisphosphate level and KCNQ currents through PI 4-kinase mechanisms. *J. Biol. Chem.* 285: 9402–9409. https://doi.org/10.1074/jbc.M109.068205

Zhang, X., X. Li, and H. Xu. 2012. Phosphoinositide isoforms determine compartment-specific ion channel activity. *Proc. Natl. Acad. Sci. USA.* 109:11384–11389. https://doi.org/10.1073/pnas.1202194109

Zong, X., M. Schieder, H. Cuny, S. Fenske, C. Gruner, K. Rötzer, O. Griesbeck, H. Harz, M. Biel, and C. Wahl-Schott. 2009. The two-pore channel TPCN2 mediates NAADP-dependent Ca(2+)-release from lysosomal stores. *Pflugers Arch.* 458:891–899. https://doi.org/10.1007/s00424-009-0690-y